Label-free, Real-time Detecting and Monitoring of Drug Dosage and Bacteria

by

Avneet Bajwa

B.Eng., Panjab University, 2007

Thesis Submitted in Partial Fulfillment
of the Requirements for the Degree of
Master of Applied Science

in the
School of Engineering Science
Faculty of Applied Science

SIMON FRASER UNIVERSITY

Spring 2012

Approval

Name: **Avneet Bajwa**

Degree: **Master of Applied Science**

Title of Thesis: **Label-free, real-time detecting and monitoring of drug dosage and bacterial**

Examining Committee:

Chair: **Michael Sjoerdsma**, Senior Lecturer, EIT,
School of Engineering Science

Ash M. Parameswaran, PEng
Senior Supervisor
Professor, School of Engineering Science

Behraad Bahreyni, PEng
Supervisor
Assistant Professor, School of Engineering Science

Edward Park
Internal Examiner
Associate Professor, School of Engineering Science

Date Defended/Approved: April 20, 2012

Partial Copyright Licence

Abstract

This report discusses the development of a miniaturized biosensor system that can be used for real-time monitoring of drug concentration and detection of pathogens in food or water samples. Conventional bacterial detection methods can take several hours or even days. This is because the bacteria need to be cultured over long periods to have large numbers of them for detection. In this report, a highly sensitive technique for counting and early detection of the growth of a colony from a single bacterium is discussed. An array of electrodes compatible with agar growth medium was prepared. A sample containing the bacteria was then cultured above the agar layer. The electrical properties of the medium were monitored using a lock-in-amplifier periodically. The data was collected using a microcontroller circuit. The variations in signal from various electrodes are compared against their initial states, revealing the presence of bacteria in the sample. This technique forms the basis of a label-free bacterial detection technique. Our technique could measure drug concentration of as low as 10pMol/mL and the detection time of bacterial growth reduced from 24 to less than 8 hours.

Keywords: pathogen detection; interdigitated electrodes; biosensor; label-free; impedance measurement; microfluidic chip; drug concentration

Dedication

I would like to dedicate this thesis to my loving parents and thank them for their unconditional love, support and care.

Acknowledgements

I would like to thank my supervisor's, Dr Behraad Bahreyni and Prof. Ash M. Parameswaran for their constant guidance and support throughout my research. Most importantly, I would like to thank them for having faith in me and encouraging me at every step of the way. Sincere thanks to Dr. Edward Park for graciously agreeing to be my examiner for my thesis defence.

Special thanks to Vidhya Ramnathan, Tim Tan, Ravindra Reddy and Shabnam for their help in the successful completion of this work. I am grateful to all my colleagues in the lab especially Sumanpreet Chinna and Alborz Amini for all of their ideas and help throughout my research.

I would like to thank Dr Timothy Beischlag for allowing me to use his lab space to carry on the experiments.

Last but not the least; I would like to thank my parents, Narinder Kaur and Hargurmeet Singh Bajwa, and my brother, Raminder Singh Bajwa and sister-in-law, Anjali Bajwa, for being a constant source of support and strength throughout my life.

Table of Contents

List of Tables

List of Figures

List of Acronyms

BioMEMS	Biological Micro-Electro-Mechanical Systems
DI	De-Ionized
ECIS	Electric Cell-substrate Impedance Sensing
FAS	Fluorescence-Activated Sensors
FEM	Finite Element Model
GPIOs	General Purpose Input/Outputs
GUI	Graphical User Interface
HPFB	Health Products and Food Branch
I/O	Input/Output
LOC	Lab-On-a-Chip
MEMS	Micro-Electro-Mechanical Systems
PCB	Printed Circuit Board
PCR	Polymerase Change Reaction
PDMS	Polydimethylsiloxane
POC	Point-Of-Care
POCT	Point-of-Care-Testing
RIE	Reactive Ion Etching
SPR	Surface Plasmon Resonance
μTAS	micro-Total Analysis Systems

1. Introduction

1.1. Background

System miniaturization has been a significant area of concern for the study of living systems, human biology and diseases, molecular and cell biology. The most commercially successful Micro-Electro-Mechanical Systems (MEMS) devices and systems have undergone a very rapid development into the field of physical sciences and biomedicine. These systems aim in providing faster, smaller, and more efficient solutions for analysis and manipulating bio-samples such as cell viability studies in drug delivery and discovery applications.

In recent years, MEMS technology has shown fast evolution in the fields of Biomedical or Biological Micro-Electro-Mechanical Systems (BioMEMS). In general, BioMEMS are systems or devices fabricated using nano or microfabrication methods for processing of biological samples. Such microsystems have been proved very useful for the analysis of drug delivery applications and for the development and processing of chemical and biological entities [1]. Consequently, many lab-on-a-chip (LOC) systems or micro-total analysis systems (μTAS) have been proposed, and these offer reliable capability of making point-of-care (POC) devices.

The field of Bio-MEMS aims at delivering an innovative platform by combining the microfluidic systems, polymer materials, surface chemistry and modification, soft fabrication techniques (including polymers and biological components). This will thereby provide biocompatibility and cost-effective solutions to biomedical problems. Therefore, it requires amalgamation of technical expertise and creativity of many engineering disciplines such as mechanical, electrical, materials and optical, with the experience of physicians and clinical laboratory scientists. In the coming years, BioMEMS devices will serve as the platform upon which nano-medicine will be delivered for the improvement of human health and disease.

1.2. Biosensors

The field of BioMEMS has attracted the highest level of research for developing POC and diagnostic systems. Such BioMEMS devices are referred to as “Biochips”. These biochips and biosensors are combined for the development of biochemical and medical applications in parallel with significant progress in these technological areas.

Biosensors can be defined as an analytical devices utilized for the detection and analysis of a bio-sample such as a tissue, microorganism, cell, enzyme, antibody or other biologically derived material for that matter. Thus, biosensor acts as a transducing microsystem, which may be electrochemical, optical, thermometric, piezoelectric, magnetic or micromechanical integrated or associated with the recognition element under test.

BioMEMS and devices have been used as biosensors and the resulting biochips can allow rapid real time measurements. These BioMEMS type of biosensors can be employed in order to detect varying drug concentration, cells, proteins, DNA, or small molecules such as lactate, glucose, glutamate, etc. [2, 3].

These biosensors usually produce an electrical signal which can be related to the concentration or the properties of a specific analyte or group of analytes. Figure 1-1 illustrates a schematic layout of the basic principles of a biosensor. According to Health Products and Food Branch (HPFB) of Health Canada, a food sample has a safety threshold limit up to which the food is good for human consumption. If the food sample has more pathogen than this threshold limit, then the quality of food is at question. Hence, detecting and counting the bacterial colonies is important to determine the quality of food sample irrespective to the location of bacterial colonies.

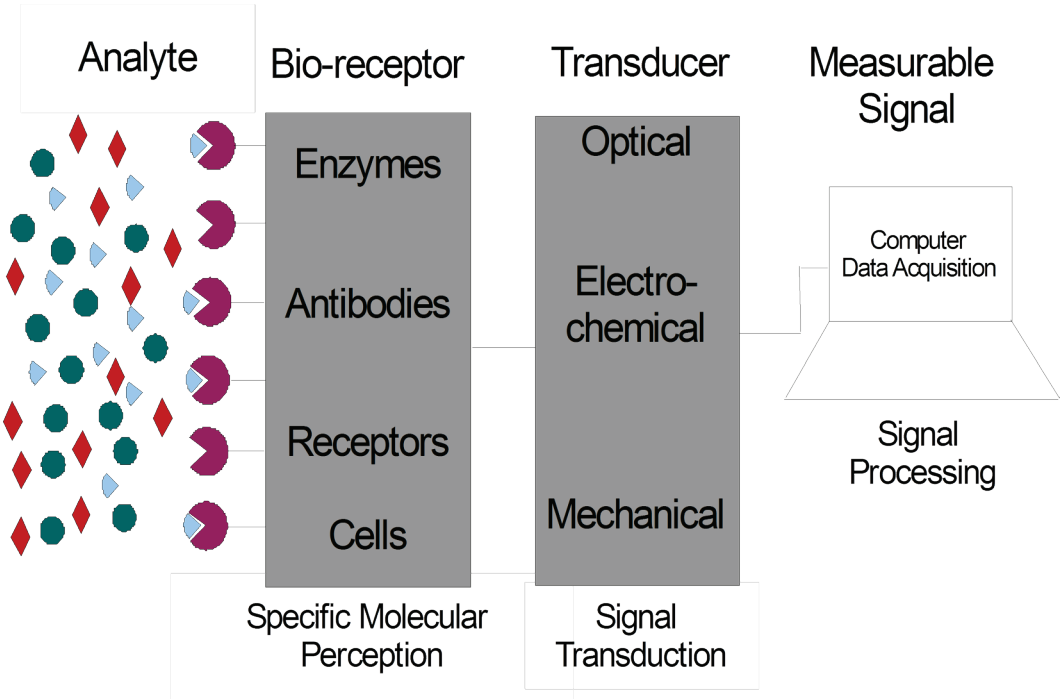

Figure 1-1: Basic principle of a biosensor

Biosensors have been developed for utilisation in a wide variety of sectors including drug discovery, medicine, food, environment, process industries, defence and security. Many detection methods such electrical, optical, mechanical are employed in BioMEMS biochips and biosensors. Each of these methods offers their own pros and cons which are discussed in Chapter 2.

1.3. Approach

1.3.1. Electrical based detection

Food safety as well as quality is a major area of concern for many decades. Nevertheless, the likelihood of contaminated food has also increased due to presence of foodborne pathogens and toxins and these pathogenic microorganisms in food lead to

severe health consequences both in animals and humans. With the concentration of food-processing plants, there is an increasing need for the development of novel and faster methods to detect these pathogens. Traditional methods, namely plate count, and PCR [4], are very selective and can be very sensitive, but at a high time cost. In fact, most of these methods may take up to a few days to yield an answer because of the multiple steps needed in the analytical process. The process of plate count involves counting the bacterial colonies after incubating them for 24 hours. PCR detection techniques are among the fastest among traditional methods. However, they are also subject to certain limitations, such as inhibition of the PCR [5], cross contamination between samples and or the ability to determine whether the detected pathogen was viable or not at the time of sampling, among others [6]. Optical detection techniques have shown a remarkable development in the field of bio- detection systems due to high sensitivity of these techniques. However, optical detection requires special labelling step, excitation source, and optics and detection circuit, making the system requirements quite laborious, complex and expensive. Moreover, the traditional plate count method cost only $15 which is much less than the cost optical lasers used for optical detection.

In this research, an electrical detection technique is devised with certain benefits over the available detection methods. The aim of this research was to detect cells present in a food sample in a shorter time span without the aid of any specialized optics or expensive hardware. The ease of use and portability of this detection technique offers aptness for in biological field applications.

To realize the electrical based detection technique, an array of electrodes was patterned on a glass substrate and the approach was to monitor the change in conduction current as the properties of the bio-sample changes due to presence of bacteria.

Initially, this sensor was used to measure minute variations in drug concentration as the plug diffuses with the buffer while it transverse in a microfluidic channel. Thus, this could be named as a chemical sensor rather than a biosensor. Computer simulations were performed to study the fluid flow in the microfluidic channels. The computer simulation results determined the system design, which, in turn, provided the

ideal fluid flow rates. The main purpose of this sensor was to determine real time variation in drug concentration with utmost accuracy. With this detection technique, we drug concentration of as low as 10pMol/mL were measured thereby justifying the sensitivity and accuracy of the sensor. The finally developed biosensor was used to detect the presence of pathogen such as E-Coli or yeast cells using the same detection technique, design of the sensor and slight variation in the set up. This could detect and predict the presence of cell colonies at a particular location within a time range of 8-10 hours.

1.4. Structure of the thesis

This thesis is divided into six chapters.

Chapter 2 provides a literature review which covers the various detection methods in BioMEMS with an emphasis on the electrical detection methods and its application in the field of Biosensors.

Chapter 3 provides the finite element simulation results for the two types of biosensors used in the research. These simulation results recommend and help in the development of a final microfluidic system design.

Chapter 4 is an in-depth explanation of the design, fabrication, packaging and testing process utilized for detecting the concentration of a drug sample. This chapter describes the process flow of the fabrication techniques for microelectrodes and Polydimethylsiloxane (PDMS) microchannels and the reactive ion etching (RIE) bonding technique.

Chapter 5 discusses in detail the design, fabrication, packaging, and testing of the microelectrode arrays utilized for detecting the bacterial growth in a food sample. It also outlines the challenges faced in fabrication and testing the biosensor.

Finally, Chapter 6 gives an insight into the future work and presents the contribution of this research.

2. Background and motivation

Many groups have been conducting research in the fields of BioMEMS and μTas (Micro Total Analysis Systems) for the development of various micro-fabricated integrated systems for preparation, separation and detection of cells. These techniques are based on either microarrays or microfluidic systems since it increases the throughput of the data and resolve smaller signals. The advantages of such systems are the micro-volumes of biological or biomedical samples that can be delivered, processed and analysed in an integrated fashion, the dramatic reduction of the required human involvement in sample handling and processing, and the improvement of data quality. This format also facilitates the reduction of overall cost and measurement time and in parallel it improves the sensitivity and specificity of the analysis.

Recently, there has been a significant increase in the field of electrical based detection techniques [7-10]. This detection method is inexpensive, straightforward and has the advantage that electrical signal can be conveniently processed and recorded in contrast to the conventional optical detection method [11]. The experimental set up is also used in ECIS (Electric Cell-substrate Impedance Sensing) studies which measure the change in impedance of a small electrode due to presence/reactions of a cell near that electrode. Applications of this technology include cell culturing [12], cell counting [13] and pathogen detection[14]. These techniques serve as a replacement to fluorescence-activated sensors (FAS) since they focus studies on cell sizing, viability as well sample concentration. Optical detection techniques have shown a remarkable development in the field of bio- detection systems due to high sensitivity of these techniques. Nevertheless, optical detection requires special labelling step, excitation source, and optics and detection circuit, making the system requirements quite laborious, complex and expensive. This thereby narrows its use only clinical laboratories and scientific research centres.

Both optical and electrical approaches have their own advantages and drawbacks. Many of the publications have presented that optical based detection techniques are highly sensitive and reliable cell detection approach [15-17]. However, optical detection techniques require cell tagging, thereby, possibly discriminating the properties of the cell and hampering the test data. In contrast, electrical based detection techniques are less expensive and label-free which leads to no cell modification and simplifies the whole set up.

Both the techniques offer integration and miniaturization of devices as the key advantage. In future, this would also allow in performing a number of operations automatically such as cell sampling, preparation, culture, and detection of cells as well as monitor varying drug concentration.

2.1. Biosensor Characterization

A number of techniques have been reported so far to characterize and distinguish different sensors. Some detection techniques compute the physical characteristics (e.g., electrical, optical, and density) of the sample under test, while others rely on markers (e.g., fluorescent and magnetic) which highlight a specific element. Although, the use of markers is a very accurate detection technique; they usually require a special labelling system that alters the properties of the constituent, example, a cell. This is particularly true for cells from the immune system, where the cell's sensitivity to various antigens is influenced in different ways [18, 19].

Apart from this, considerable amount of time is required in order to tag the molecule to its target depending on the concentration, diffusion properties and position of the constituent. Use of microchannels or integrated mixers can significantly reduce the diffusion time in small chambers providing a reaction in a fraction of the time necessary with a standard test tube. In some cases, an additional problem is that some non-surface markers need to enter the cell membrane in order to reach their specific target. This often requires a membrane permeabilization step, which affects further analysis performed on the cell. A number of optical detection based microsystems are

reported for analysis and cell sorting application [20]. These systems are very promising for the development of commercial devices in future.

For some applications, where the intrinsic optical properties of the particles under analysis are such that they exhibit auto-fluorescence, labelling is not necessary. A common example of this is the study of phytoplankton algae that contains different photosynthetic pigments. In order to identify various species, emitted light upon excitation with different laser wavelengths is measured [21].

Another approach is miniaturized electrical techniques, mainly based on either AC electrokinetic or impedance spectroscopy techniques [22], which is discussed in detail in this chapter. Both approaches are label-free and less expensive techniques as compared to optical detection techniques. Electrical detection techniques measure specific properties of cellular sub-structures such as the cell membrane, cytoplasm, or nucleus at distinct frequencies due to variation in dielectric properties and dimensions of the cell.

Dielectrophoretic separation can be achieved by selecting a frequency where the amplitude or direction of the applied forces are sufficiently large to push, hold, or detect a specific cell type while leaving other cell types unaffected. Electro-rotational measurements of cell properties are generally done by video analysis of the rotational speed of a cell subjected to a rotational electric field over a range of frequencies. AC electrokinetic experiments are generally done in low conductivity saline in order to enhance the range of forces that can be applied and reduce Joule heating effects. The applied electric field is generally less than 10^4 Vm^{-1} but can reach up to 10^6 Vm^{-1} at the MHz frequency range, without damaging the cells to the great extend. In the lower frequency range, where the cell membrane polarizes more easily, electro-permeabilization treatment or electro-bursting of cells can occur for electric field strengths around 10^5 Vm^{-1} [23, 24].

In dielectric spectroscopy, electrical properties of a cell suspension are measured using very minute volumes [25-27]. To obtain a reasonable signal and limit particle-particle interaction, the volume fraction of particles in suspension is typically in the range of 1-30%. Still, even in such cases where a small volume and small volume

fractions are used, the resulting measurement gives an average over a large number of cells. This represents a significant drawback of such systems as the discrimination of cell sub-population and cell sorting is impossible. To address these issues, microsystems can be used in order to define microscopic detection zones by defining a pattern of microelectrodes within the microchannels. Cells can then be studied individually in a sequential manner rather than in bulk. The parameters primarily accessed using this technique are the cell volume, cell membrane capacitance, and conductance, as well as electrical parameters related to the cytoplasm [25-27].

2.2. System platform and integration

The integration on a microsystem platform along with several complementary tools is a challenging goal, which opens up an area of possible applications for this technology. A number of groups have demonstrated optical and electrical means for cell manipulation and analysis in microfluidic devices. Over the last couple of years, this technology has significantly been improved to build robust analysis systems. The development of these new techniques, such as cell bursting and single-cell genetic modification, achievable in integrated systems by the use of electro-mediated lysis of cells and electro-permeabilization, is opening up the field and will lead to a plethora of novel diagnostic devices in the coming years.

Although significant progress has been made in developing these miniaturized manipulation and diagnostic systems, generally these samples are to be processed off-chip using lengthy, labour-intensive preparation methods. Proper sample preparation is especially important, which may cause obstruction of the system's microfluidics and result in failure of device operation. The use of filters and other cleaning techniques solved these problems to a great extend; still, achieving good results relies heavily on the initial sample preparation.

Automation with laboratory and control via computer play equally important roles. In order to have results beyond the proof of concept a good degree of repeatability, both in processing samples and monitoring controlling parameters is required. Automation in processing the acquired data is also necessary and permits one to rapidly detect any problem with the system operation and apply corrective steps.

2.3. Detection techniques

2.3.1. Optical Detection

The chip substrate consist of optical quality glass, it is therefore possible to perform optical measurements on the cells as they pass through the channel. Details of such an optical system are shown in Figure 2-1. This system was designed to measure fluorescence from single cells at three different wavelength ranges. To optically excite the cells, light from 532 nm (solid state YAG) and 633 nm (HeNe) lasers is coupled into the channel using a free-space optics setup and a standard microscope objective. The laser beams are combined and pass through a beam expander into infinity corrected objective lens or detection the fluorescent light emitted from the cells is collected by the same objective lens is spectrally and spatially filtered by passing through dichroic mirrors, band pass filters, and lens and pinholes positioned in front of photomultiplier tubes (Hamamatsu). The intensity of the light at the focal point of the objective (optical detection zone in the channel) is typically 600 μW. The emission filters have centre wavelengths of 585 nm and 675 nm and a long pass filter with cut-off at 710 nm (Chroma, Buckingham, VT, USA).

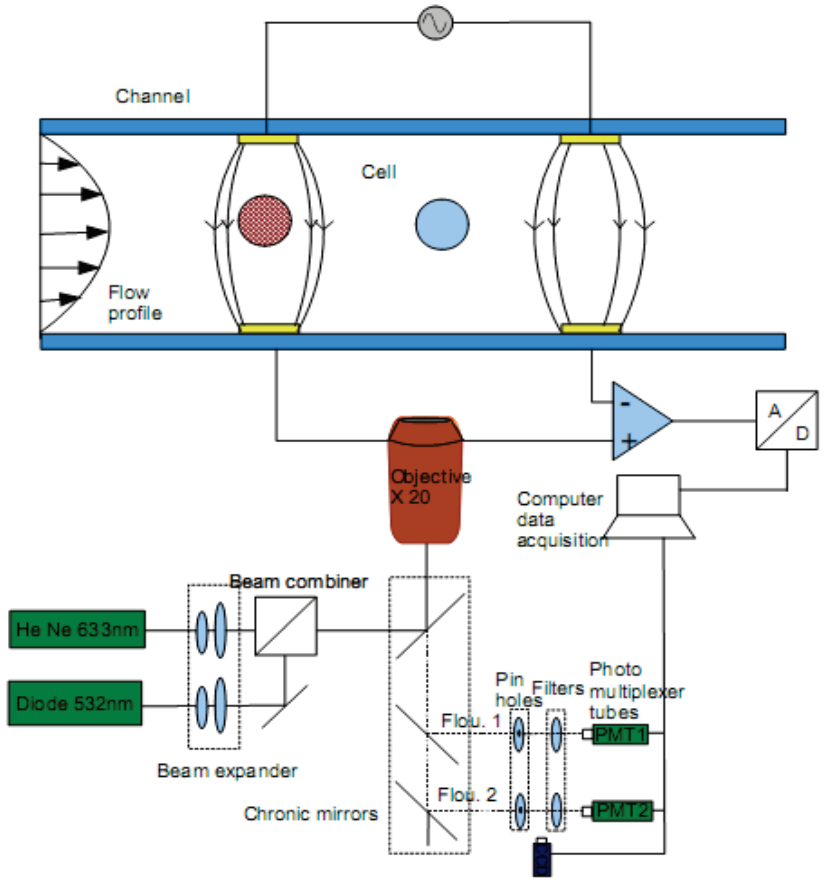

Figure 2-1: Schematic of a single-cell optical detection using two excitation lasers and up to three emission detectors.

2.3.2. Detection using impedance measurement technique

The most commonly used method of sizing and counting particles is the coulter method which is based on measuring the changes in electrical resistance produced by cells or particles passing through the small aperture as shown in Figure 2-2 [28]. In this technique, current is generated by the two large electrodes placed parallel to each other and voltage is measured as the particle passes through the aperture. This measured voltage as the particle passes through the aperture is proportional to the volume of the particle. Several thousand particles per second can be individually counted and their size can be determined. In addition, a metering device is used to draw a known volume of the suspension through the aperture; a simple count of the number of pulses can then

yield the concentration of particles in the sample. In applications such as peripheral blood differential leukocyte count, statistic sizing is generally sufficient to detect different types of cardiomyocytes [29]. Forcing both the electrical current and the cell stream into a small aperture is a simple method to generate a highly sensitive detection volume to achieve single-cell detection. As a first approximation, the sensitivity of the measurement increases with the selection of a smaller diameter. The limit is that the aperture has to be big enough to accommodate the passage of the largest particle in the suspension.

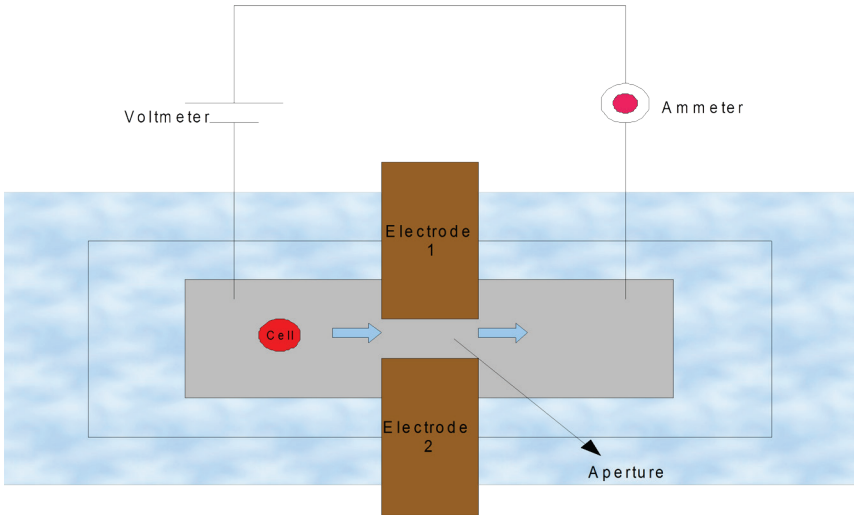

Figure 2-2: Impedance based detection using coulter method

2.3.2.1. On-Chip Examples

The first µCoulter devices were proposed by *Larsen et al* [29] and *Koch et al* [30]. These systems were microfabricated in silicon and used microfluidic microchannels and filter structures. Reports of on-chip measurement by *Fuller et al.* on granulocytes [31], *Larsen et al.* on somatic cells using a simple silicon aperture [32] and *Gawad et al.* on erythrocytes using a coplanar electrode geometry [33] have already been reported. The original µCoulter technique is limited to cell sizing by the use of a single measurement frequency, generally at low frequency or DC. However, measurement at multiple frequencies is necessary to determine other attributes of the cell, similar to what

is obtained in traditional dielectric spectroscopy. *Ayliffe et al* presented an integrated cytometer device for stop-cell measurements using a frequency sweep on electroplated gold electrodes [22].

2.3.2.2. Coulter Measurement

The electric field geometry is a very important aspect of the system since is directly related to the shape and amplitude of the detected impedance signal. According to *Deblois*, the variation of the resistance '∇R' due to a small particle of diameter 'd' passing in an aperture of diameter 'D' is given in first approximation as

$$\Delta R = \frac{4\rho r d^3}{\pi D^4} \text{ as } D^4 \alpha J^{-2} \text{ then } \nabla R \alpha \rho d^3 J^2 , \qquad (1)$$

where J is the current density in the tube section. Considering this physical aperture as a current tube, it can be seen that the amount of information gained from a specific location by impedance measurement using a bipolar electrode configuration is proportional to the square of the local current density.

Consequently, some of the important differences that exist between on-chip cell impedance analysis and the traditional Coulter instrument are related to the use of microelectrodes and micro fluidic geometries to define the shape of the electric field geometry. As mentioned above, in the Coulter example, the measured electric field is produced by relatively large electrodes on each side of a small aperture. This approach offers some significant advantage at low frequency due to the increased electrode surface area and reduced impedance of the electrode/electrolyte interface. By reducing, the device dimensions to it the system in a microfluidic chip, two possibilities or levels of integrations may be considered.

Firstly, the size of the electrodes can be kept relatively large (200 × 200 μm^2 range) and use a micro-fabricated aperture or a constriction in the channel section. This approach requires careful analysis of the inhomogeneous distribution of the current density at the electrode surface. This effect, especially in the case of shallow channels can significantly reduce the electrode effective area. In the case of impedance spectroscopy at frequencies up to 20 MHz, large electrodes can also lead to higher stray

capacitances and limit the sensitivity for high frequency measurements. Integration of other systems such as cell tracking and sorting with practical cell dilutions (10^6 ml^{-1}) will be more difficult due to the larger volumes of liquid in the system. In a sandwich structure, electrodes patterned only on the bottom side of the channel may be used. In addition, a certain distance must be set between the electrodes and the constriction or aperture of approximately three to five times the channel height; this is to establish a homogeneous electric field in the vertical direction.

Secondly, it we can further reduce the size of the electrodes down to the characteristic dimension of the cells or particles under study, which has several implications. In this case, the detection area is directly defined by the electrode geometry within the capillary channel. This approach reduces stray capacitances and thus increases the device operating bandwidth toward higher frequencies. Small channel cross-sections permit sequential tracking of cells along the channel and the integration of features such as sorting by partitioning the channel length for successive operations. Small microelectrodes result in an apparent dilemma; on the one hand, a higher sensitivity results from the higher field line concentration around the cell. On the other hand, the high interface impedance (due to the electrical double layer) makes measurement at low frequency more difficult. To alleviate this problem there are some techniques to increase the effective surface area of microelectrodes based on nonporous films such as platinum black, iridium oxide, or titanium nitride [34, 35].

Another issue arises from the inhomogeneous current density, either be it within the channel constriction (i.e., aperture) or if small electrodes are used between the closely placed electrode pair. This in homogeneity can bias the detection signal peak, as a function of the particle's trajectory, as it passes through the measurement volume. In traditional Coulter systems, the length and shape of the aperture plays an important role in controlling the uniformity of the signal shape and this has been extensively studied[36]. Similar studies may be performed for the integrated chip approach with embedded microelectrodes. A complex dielectric model is used to determine the change in electric current between a pair of electrodes due to passage of a biological cell. The influence on the dielectric spectrum of different cell properties, such as membrane capacitance and cytoplasm conductivity is of particular interest. The measurement volume is located between a pair of facing microelectrodes in a microchannel filled with

a saline solution. A 3D finite element model is used to determine the electric field in the channel and the resultant changes in charge densities at the measurement electrode boundaries as a cell lows through the measurement volume. The charge density is integrated on the electrode surface to compute the displacement current and the channel impedance for a given applied alternating electrode voltage and frequency. The excitation signals are taken to be of suitably low frequency and low applied voltage, allowing the quasi-static approximation and linear behaviour of the system to be assumed. In the present example, the measurement volume geometry details are for the specific case of a sensor with a channel of 20 × 20 μm^2 cross-section and two facing electrodes, 20 × 20 μm^2 in area, on opposite walls of the channel as shown in Figure 2-3.

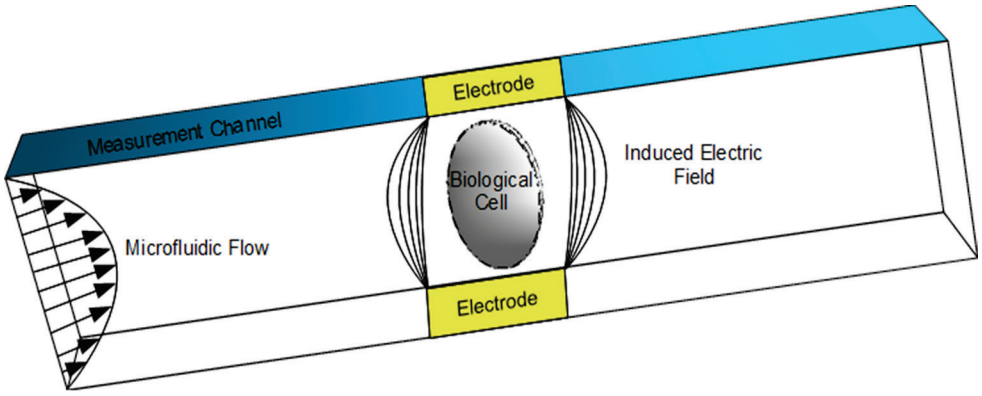

Figure 2-3: Diagram of flow cytometry measurement in a microchannel with integrated microelectrodes. [37])

These channel dimensions are chosen in order to determine the sensitivity of a sensor, which could accommodate cell diameters up to 15 μm without clogging the channel.

A dielectric sphere of equivalent complex permittivity is used as a simplified model to describe a biological cell. The model includes various geometrical parameters of the cell, such as size and position in the channel. Using such a model it is shown that given a reasonable size and placement of the cell along the centre line of the channel, good signal reproducibility can be obtained. Also using analytical methods, such as

conformal mapping, compensation factors can be found, depending on the sensor geometry, to account for the fringing effect and non-uniformity of the electric field. Numerical approaches have been used to determine the practical limits of this compensation method [37].

2.3.2.3. Differential Measurement

In practice, the measurement area of the chips contains two measurement areas (pairs of electrodes) in close proximity. In the measurement area, the channel width is reduced in order to decrease the detection volume and thus increase the electrical sensitivity of the system to the passage of the cell. This restriction also decreases the chance of having two cells entering the measurement area simultaneously. The electrode areas are typically 20 x 40 μm^2 and channel cross-section 20 x 40 μm^2. The distance between the two electrode pairs is 60 μm.

The particle or cell moving under pressure-driven low successively pass through the two electric field regions, thus consecutively modifying the current through each detection volume. The use of a differential measurement scheme significantly reduces the measurement noise; small thermal fluctuations or variations in the composition of the suspending fluid are thus cancelled out. The chip is connected to a circuit, which uses differential electronics to amplify the small difference of current passing through the two sensors. This approach allows rejection of the common mode signal early on, avoiding saturation of the amplifiers. A double peak (one positive and one negative) electrical signal shape is thus obtained for each passing cell (Figure 2-4). This approach offers many advantages compared to a non-referenced measurement technique in terms of ground level stability and signal amplification. The cell speed within the detection channel is obtained by dividing the centre-to-centre distance between the detection volumes by the transit time t_{tr} separating the two measured peaks. This method also presents some advantages in terms of robustness compared to a single peak width measurement, as it is less sensitive to the cell size or shape.

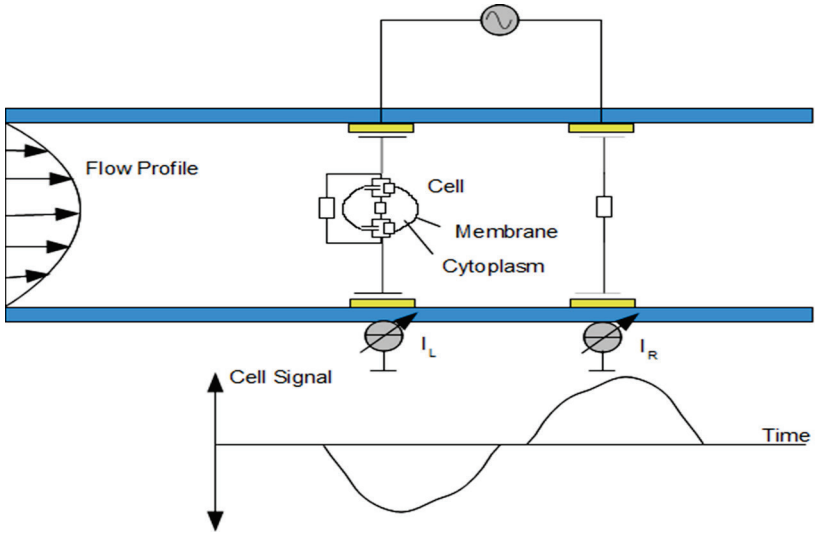

Figure 2-4: Cell detection principle and expected electrical differential current signal for a passing cell. The detection and reference volumes switch as the cell passes through each. The bottom electrodes are kept at a virtual ground potential [38]

2.3.2.4. Guard Ring

The addition of a guard ring in order to straighten the electric field lines around the current sensing electrodes is a practical approach that addresses the issue of the electric field uniformity and permits simplification of the calculation of the cell geometric factor. The use of grounded guard electrodes in conjunction with current sensing electrodes connected to a virtual ground in auto-balanced bridge configuration is preferred (Figure 2-5). This is because at higher frequencies (MHz and greater) it is difficult to implement non-phase lagging followers to drive active guard electrodes, as would be required by a traditional bridge electrical circuits. This amplification approach also reduces the effect of the stray capacitances, as there is no current leakage from the current sensing leads, at a virtual ground potential, to the ground shielding or guard electrodes leads.

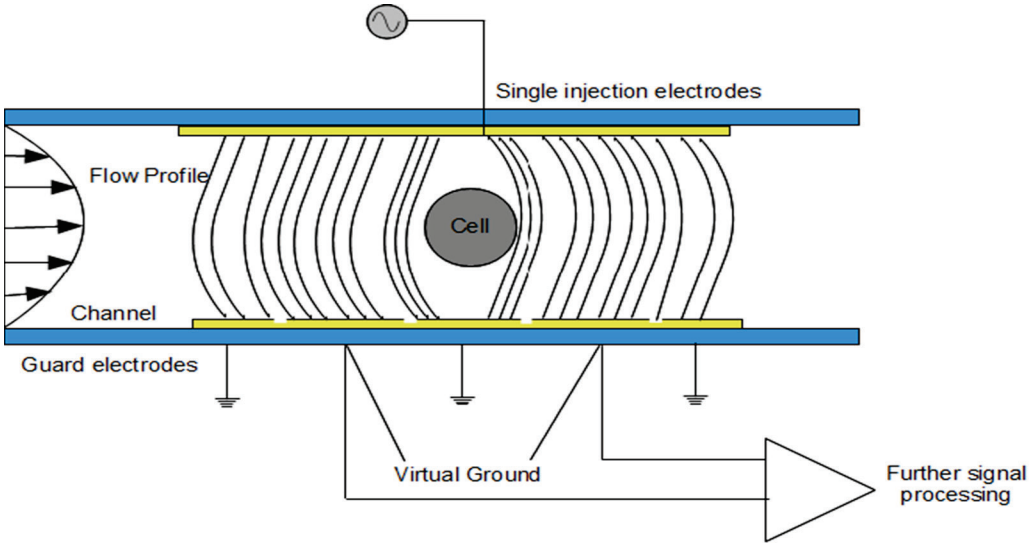

Figure 2-5: Principle and geometrical approach to implement guard electrodes in a differential auto-balanced amplification scheme.

2.3.2.5. Point Differential Electrodes

An alternative method to that of nano-porous modification of electrodes surfaces, to increase the effective charge density of the electrodes, is the use of a 4-point differential electrode configuration [39]. In this configuration, an alternating voltage applied between two large microelectrodes placed at either end of the channel and the injection current is measured. Three pickup electrodes are placed symmetrically in the channel. The differential voltage drops between the pickup electrodes are then amplified and compared yielding the impedance variation due to the presence of the cell. Impedance variation is measured at low frequency (1-2 kHz) for the passing cell as a function of its position in the channel.

The pickup electrodes surface capacitance, due to the double layer, still subsists in the tetra-polar measurement scheme. However, since the input impedances used in the amplification is high only negligible amounts of current flow through those electrodes. The measured transient changes in voltage at the electrode thus correspond to those taking place in the liquid bulk with minimal voltage drops due the double layer capacitance.

3. Finite element modelling

In many drug delivery systems, it is very crucial to release a drug at a predetermined rate by maintaining a constant concentration level for a specified period of time. Thus, determining the concentration profile of a sample drug is one of the principle areas of interest for drug delivery and discovery systems, drug dosage planning, and antibiotic susceptibility studies of cells [7, 36, 37]. The primary target application of this study is drug development for cardiovascular diseases where the response of heart cells to specific drugs needs to be studied. A recent development in the area is based on measurement of the mechanical response of the cells to various drug concentrations, which in most cases are ionic solutions [38]. The current experimental setup is based on exposing a single heart cell to a known concentration of a drug while measuring its contraction forces. This method requires delivering a specific dose of the drug for a relatively short period of time. However, the exact drug dosage is difficult to control for rapid variations in drug concentration, which negatively affects the accuracy of the measurements. In this chapter, finite element model (FEM) simulations are discussed to study the fluid flow in the microfluidic channels. The computer simulation results helped in determining the system design, which, in turn, provided the ideal fluid flow rates. However, the main purpose of these simulations was to determine real time profile of the variation of drug concentration.

3.1. Model definition for pressure driven flow

In the first section of this chapter, a study of a pressure driven flow for a cross microchannel was conducted in finite element (FE) simulations using COMSOL Multiphysics® [44]. These simulations were performed before fabricating the sensors to find the geometry of the microfluidic chip, flow velocities of the buffer and the sample, and to study concentration profiles of the sample drug over time. The horizontal channel serves as the loading channel while the vertical channel is the dispensing channel. The

actual model was simulated in 3D with rectangular geometry dimensions as tabulated in Table 3-1.

Table 3-1: Dimensions of the simulated model

	Width	Length	Depth
Loading Channel	50 µm	1cm	100 µm
Dispensing Channel	50 µm	3cm	100 µm

Finite element analysis of the device operation is divided into three stages:

- Creation of a plug
- Correlation of concentration of the injected plug with admittance
- Analysis of the effect of cell
    - Cell orientation
    - Electrode configuration and input frequency

These three steps are explained below.

3.1.1. Creation of plug: loading and dispensing stage

In the loading stage, a drug sample having a determined molar concentration in mol/m^3 was loaded into the micro-fluidic channel through the top vertical channel at a particular flow rate. Buffer was injected from the two horizontal ends of the channel so as to ensure a plug formation. At the dispensing stage, the supply of the drug sample was stopped and buffer was injected into the channel which causes the sample at the intersection of the channel to be pushed into the horizontal channel. Drug loading and dispensing stage are as shown in Figure 3-1.

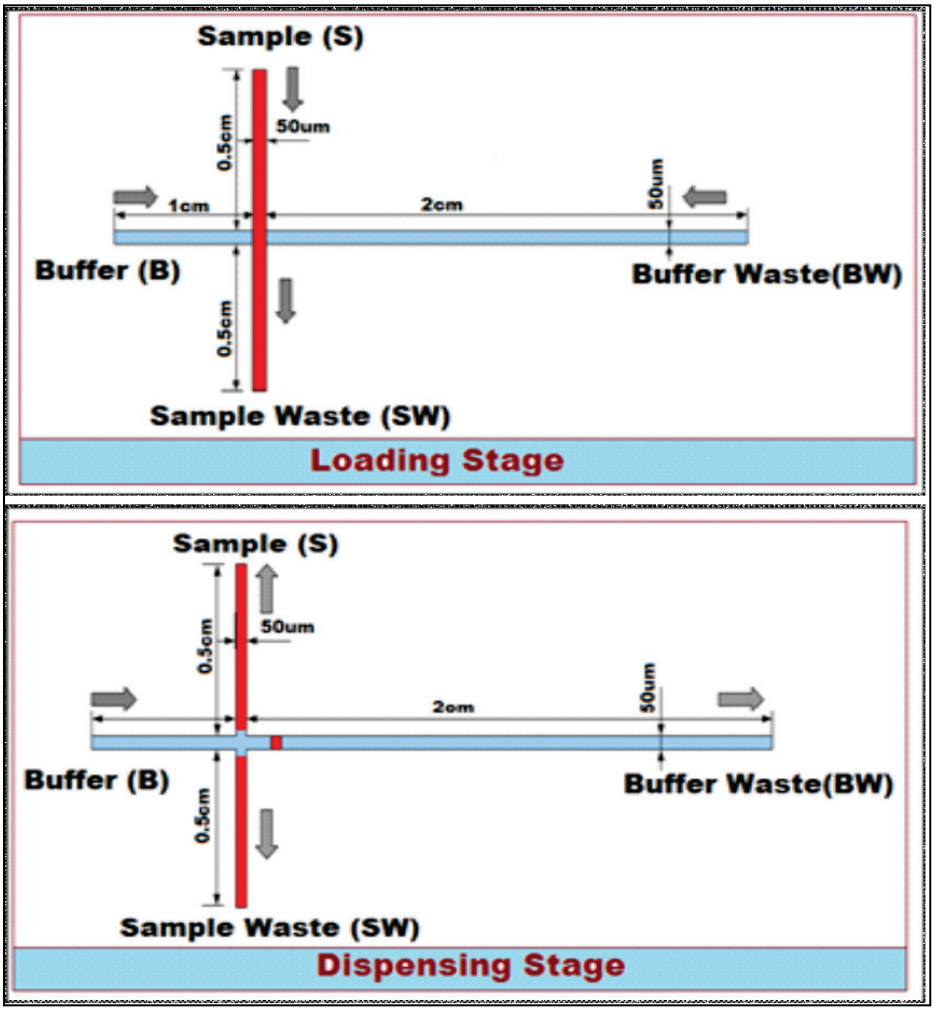

Figure 3-1: Drug loading (top) and dispensing stages (bottom)

In this model the steady-state solution for the loading stage was used as the initial condition for the transient analysis of the dispensing stage.

The following application models of COMSOL Multiphysics® [34] are utilized and solved sequentially with a nonlinear solver in the following order:

- Incompressible Navier-Stokes

$$-\nabla.\eta(\nabla u - \nabla u^T) = 0 \qquad (2.1)$$

$$\nabla u = 0 \qquad (2.2)$$

- Convection and diffusion

$$-\nabla(-D\nabla c + cu) = 0 \quad (3)$$

- Nernst Plank

$$\nabla(-D\nabla c - zuFc\nabla\emptyset + cu) = 0 \quad (4)$$

where,

ρ = density, 1000 (kg/m^3)

u = velocity (mm/s)

σ = conductivity, 5.5X10^{-6} (S/m)

η = viscosity, 0.001 (Pa.s)

D = diffusion coefficient, 2 X10^{-10} (m^2/s)

c = concentration, 2.65Molar

z = charge number, +1 & -1

T = Temperature, 298K

F = Faraday's constant, 0.0 6354 (kg/mol)

Φ= Potential (V)

The boundary and subdomain conditions of the loading and dispensing stage are tabulated in Table 3-2.

Table 3-2: Boundary and subdomain conditions of the loading and dispensing stage

	Loading Stage		
	Incompressible Navier-stokes	**Nernst Plank**	**Convection and diffusion**
Subdomain settings	ρ =1.0×10^{3}Kg/m^3, η= 1×10^{-3} Pa.s, ε_r= 80.2 and mean free path=1×10^{-6} m	Conductivity, σ= 5.5 × 10^{-6} S/m Diffusion coefficient,D=2 ×10^{-10} m^2/s z = charge number, +1 & -1 Mobility = 8×10^{-14} (s.mol/kg)	Diffusion coefficient,D=2 ×10^{-10} m^2/s
Boundary conditions	All the boundaries except the reservoir boundaries are set as *wall* with *No slip.* The reservoir boundaries are set as Sample(S) = 60mm/s, Sample waste(SW) = *Zero pressure and no viscous stress* , Buffer(B) & Buffer waste BW= 20 mm/s	All the boundaries are set to *Electric Insulation.*	All the boundaries except the reservoir boundaries are set to *Insulation/symmetry.* The reservoir boundary are set to *Concentration* with following values; Sample(S) = 2.65M, Sample waste(SW) = 0, Buffer(B)= 0, and Buffer waste(BW) = *Convective flux*
	Dispensing stage		
Subdomain settings	Remain the same as the Loading stage		
Boundary conditions	Remain the same as the Loading stage, only the concentration value at Sample(S), Sample waste (SW) and Buffer (B) are changed to zero and Buffer waste (BW) is set to *convective flux*. The values of the flow velocities are changed to Sample(S) = -0.04mm/s, Sample waste (SW) =-0.04 mm/s, Buffer (B) = 0.4mm/s, and Buffer waste (BW) = *Zero pressure and no viscous stress*.		

3.1.2. Correlation of concentration of the injected plug with admittance

Impedance based detection is a rapid, inexpensive technique. Traditionally, impedance method used thin metal wires as electrodes for impedance measurements [45]. In recent years, MEMS based interdigitated array microelectrodes (IDAM) are being used. The combination of a microfluidic flow cell with IDAM enables high sensitivity, handling small volume and rapid detection. In this section, we report the simulation of the electrical impedance of an IDAM based concentration profile measurements and the various factors that influence the impedance.

Admittance (Y) is the inverse of the impedance (Z) and it is expressed as

$$\underbrace{Admittance}_{Y} = \underbrace{Conductance}_{G} + j\ \underbrace{Susceptance}_{B} \qquad (5)$$

Most of the simulation results discussed here will consider the real part of admittance i.e., conductance in equation 5. The model was simulated in 3D and uses the electric currents time–harmonics analysis application mode of the electomagnetics module in COMSOL Multiphysics® [34]. The unknown field quantity calculated from the potential V = V(x,y,z), a complex valued quantity. The solution of the dispensing stage was stored to be used as an initial condition for this set of simulations. The applied boundary and subdomain setting are tabulated in Table 3-3.

Table 3-3 : Boundary and subdomain conditions correlation of concentration of the injected plug with admittance

	Incompressible Navier-Stokes	Electric currents	Convection and diffusion	Nernst-Plank
Subdomain settings	$\rho = 1.9\times10^{3} Kg/m^{3}$, $\eta = 1\times10^{-3}$ Pa.s, ε_r= 80.2 and mean free path=1×10^{-6} m	$\sigma = 5.5\times10^{-6}$ S/m, ε_r=80.3	Diffusion coefficient, $D=2\times10^{-10}\ m^2/s$	Mobility $\mu_m = D/(R_g*T)$, where, $D = 2\times10^{-10}\ m^2/s$, R_g= 8.314 J/(mol*K) T= 298 K
Boundary conditions	All the boundaries except the reservoir boundaries are set as *wall* with *No Slip*. The reservoir boundaries are set as S &SW = -0.04 mm/s, B= 0.4 mm/s, and BW= *outlet with No pressure, no viscous stress*	All the boundaries are set to *Electric Insulation except the electrodes.* Electrode1= *port as input 0 (forced voltage)* and electrode 2 = *ground.* Frequency of the signal is set to be 50 Hz.	All the boundaries except the reservoir boundaries are set to *Insulation / symmetry.* The reservoir boundary are set to *Concentration* with following values; S,SW &B = 0,BW= *Convective flux*	All the boundaries are set to Electric Insulation

There is pair of gold electrodes at the right side of the channel. The electrodes are defined to be 50μm long and 10μm wide with an inter-electrode spacing of 40μm. Simulations are done by placing the electrodes at two different locations from the intersection of the channels: 200μm and 600μm (Figure 3-2).

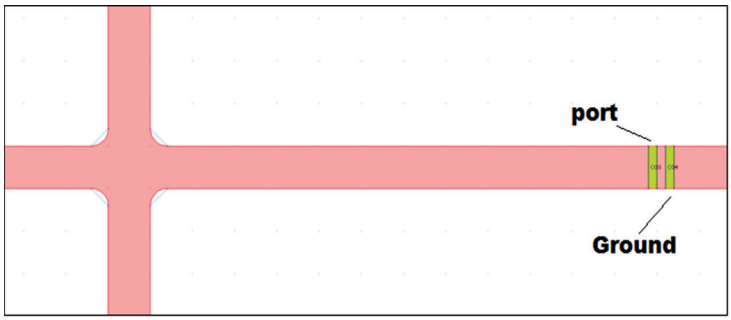

Figure 3-2: Electrode placement from the intersection of loading and dispensing channel

3.1.3. Analysis of the effect of a cell

Most of biosensors employed for detection of pathogenic bacteria are label-dependent immunosensors which are based on labelled secondary antibodies. Label-free biosensors [42] and surface plasmon resonance (SPR) [43] offer attractive advantages like speed and straightforwardness of operation. As previously mentioned, impedance based detection is another fast and low-priced choice to build label-free biosensors. This method of bacteria detection is based on the changes in the electrical properties of a medium (buffer) where bacteria cells are cultured. These changes occur due to the release of ionic metabolites from live cells which are measured by electrodes in contact with the medium [44, 45].The most frequent characterization of this technique involves observing over time the ac impedance of a pair of electrodes submerged in the buffer. If the impedance change crosses beyond a certain threshold, a positive detection is suggested. The ions given up by bacteria cells into their surroundings are either due to energy metabolism (catabolism) and/or ion exchange via the membrane [45]. This exchange helps to control the membrane potential, and the osmotic difference between the exterior and interior of the cell. In addition, biological cells comprise of adjacent structures of materials that have very dissimilar electrical properties and show large

induced boundary polarizations that are greatly reliant on the applied field frequency and their physiological states. For instance, the cell membrane comprises of a very thin lipid bi-layer having many proteins and is extremely insulating with a conductivity of around 10×10^{-7} S/m, while the cell interior consists of many dissolved charged molecules, resulting in conductivity as elevated as 1 S/m [46, 47]. Upon death, the cell membrane becomes permeable and its conductivity increases by a factor of 10^4 because of the cell contents exchanging material freely with the external medium through the membrane hence, a difference in conductivity response and a selective separation can be achieved between live and dead cells [46, 47].

3.1.4. Model approximation

For analysis of cell simulations, the electrodes were set as perfect conductors and were regarded as equipotential surfaces with zero thickness. These approximations are valid because the real electrodes are only ~0.5μm thick and the electrode material is gold with no major field dilation across the surfaces of the electrodes (i.e., every point on the gold electrode surface will have the same phase angle). This approximation reduces the complexity of the model considerably and requires fewer elements to accurately simulate the admittance between the electrodes, leading to lower memory requirements and faster computation times. Also, with this approximation the edge effects from the vertical sides of the electrodes can be ignored. Furthermore, when compared to the buffer conductivity ($\sigma = 5.5\times10^{-6}$ S/m) the conductivity of the gold electrodes ($\sigma = 4.52\times10^{7}$ S/m) can be assumed to be almost unlimited. The electric currents application mode was used in modeling cases where the magnetic inductive effects can be neglected and only resistive-conductive and electric-capacitive effects were accounted for. This approximation works better for lower frequencies and the small scale devices. The accuracy of the electric currents approximation is determined by the characteristic length scale δ called the skin depth [52]

$$\delta = \sqrt{\frac{2}{2\pi f \sigma \mu_0 \mu_r}}$$

where f is the frequency (Hz), σ is the electrical conductivity, μ_o is the magnetic permeability of vacuum and μ_r is the relative permeability. The skin depth is a

characteristic penetration depth of the surface current sheet. When the skin depth is larger than the device modeled, the magnetic or inductive effects can be neglected. In this model, at 50kHz the skin depth for the buffer is ≈3918.124km and the skin depth of the modeled gold electrode is ≈1.0cm which are significantly greater than their respective dimensions in the model.

3.1.5. Model design and assumptions

The model consists of a 50μm cuboid. The cube is filled with a buffer of conductivity 5.5×10^{-6} S/m and a relative dielectric constant of 80.3. These are the standard values for de-ionized water [50]. The sides of the cuboid confine the buffer volume. The boundary condition on all six sides of the cuboid are set to electric insulation. The sample cell is defined as an ellipsoid of dimension 10μm × 3μm × 3μm. The conductivity and relative dielectric constant of the sample cell is set to be 1S/m and 60 respectively [50, 51] and upon death, the cell conductivity is considered as 10×10^{4} S/m. The cell/cells are placed at a height of 10μm from the electrodes. Figure 3-3 shows the geometry of the model. Table 3- 4 tabulates the boundary and subdomain settings.

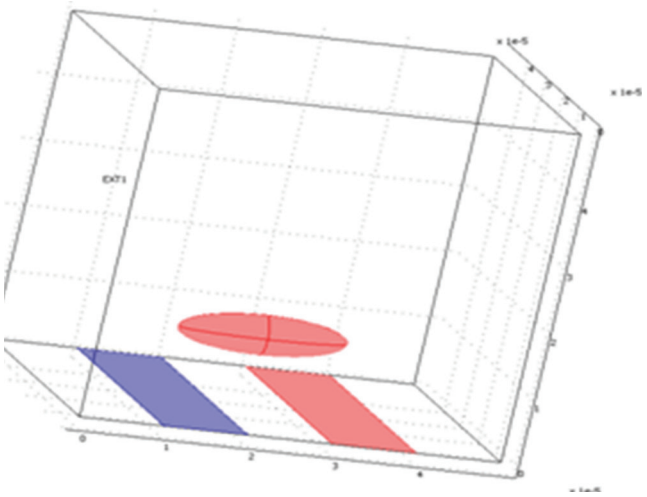

Figure 3-3: Geometry of the model, showing the cell and the electrodes

Table 3-4: Boundary and subdomain settings for cell analysis

Electric currents	
Subdomain1(The environment of cell)settings	$\sigma = 5.5\times10^{-6}$ S/m, $\varepsilon_r=80.3$
Subdomain 2 (The cell) settings	$\sigma_{alive} = 1$ S/m, $\varepsilon_r=60$ $\sigma_{dead} = 10^4$ S/m
Boundary conditions	All the boundaries are set to *Electric Insulation* except the electrodes and the cell boundaries. Electrode1= *port as input 0.5V (forced voltage)* and electrode 2 = *ground.* Frequency of the signal is set to be 50 Hz. The cell boundaries are set to *Distributed Impedance* with $\sigma_{alive} = 1$ S/m, $\varepsilon_r=60$, $\sigma_{dead} = 10^4$ S/m

3.2.Simulation results

3.2.1 Loading stage

In the loading stage sample drug was inserted into a vertical channel at a particular velocity and the buffer is injected through the two ends of the horizontal channel. This causes the concentration to be focused in a very narrow thin region at the intersection of the loading and dispensing channel. The two different sets of boundary conditions are simulated to determine the best set for the loading of the sample with given channel dimensions and conditions. Figure 3-4 shows the concentration distribution at the intersection of two channels in the middle of horizontal channel. For velocities 60mm/sec and 20mm/sec of the sample and the buffer, respectively, the plug had the ideal concentration profile within the dimensions of the intersection area. But it is observed that as the buffer velocity is increased the maximum concentration in the intersection of channels also decreases due to the mixing of buffer and sample. In order to increase the molar concentration of the plug, the initial molar concentration of the

drug/sample can be increased to get desired concentration of drug to be injected into the horizontal channel.

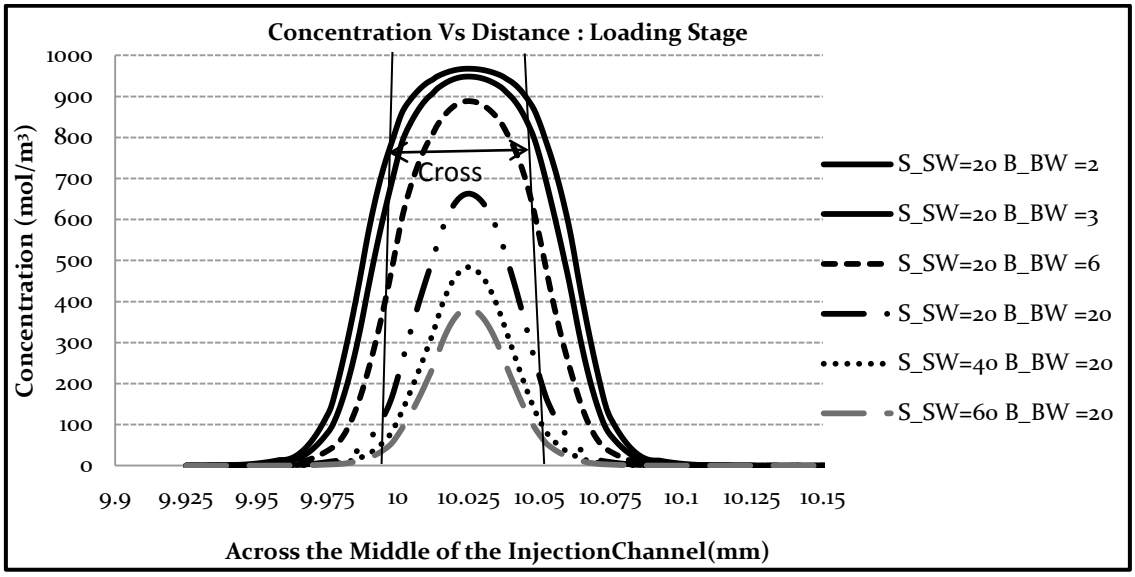

Figure 3-4: Finite element simulation results for the determine concentration profile at the middle of the channel at various boundary flow velocities

The ionic conductivity profile obtained for the same velocities is as shown in Figure 3-5.

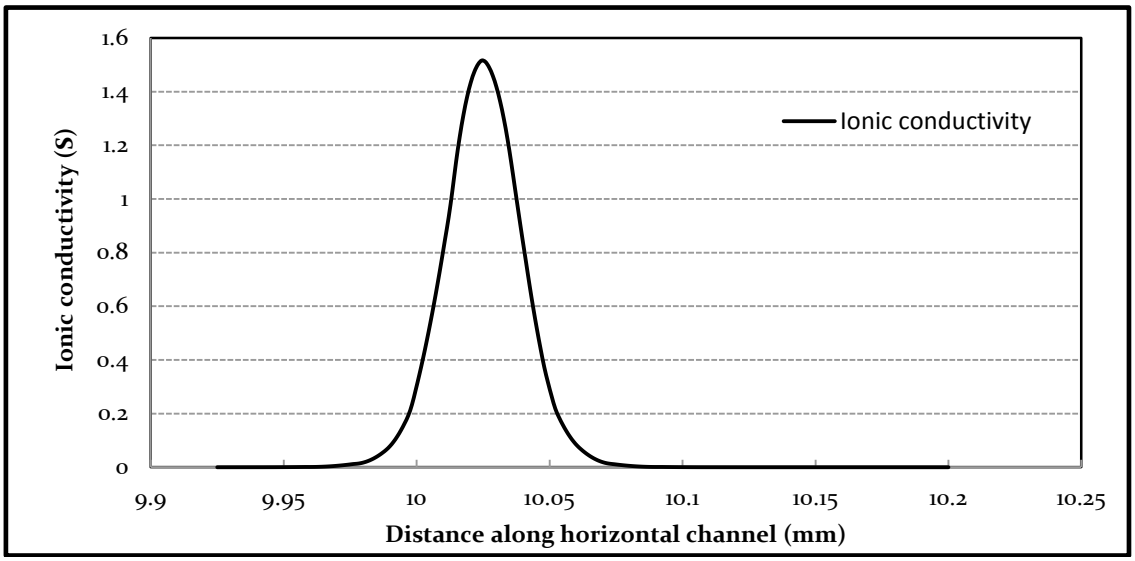

Figure 3-5: Ionic conductivity profile at the middle of the channel at drug velocity=60mm/sec and buffer velocity=20mm/sec

It is evident from Figure 3-5 that as the concentration changes the ionic conductivity follows the same trend as the number of ions behaves in the similar way.

3.2.2 Dispensing stage

In the dispensing stage, a trade-off was observed between the distance a plug travels in the dispensing channel and the amount of sample pull-back that occurs in loading channel. Greater pull-back of the sample resulted in compromised progression of the plug in the loading channel and vice versa. Also, if the velocity of the buffer was increased then the plug travelled a longer distance but it also diffused more and vice versa. The progression of plug at time 0 to 10 sec at a buffer velocity of 0.3mm/sec is shown in Figure 3-6. Figure 3-7 illustrates the ionic conductivity of the travelling plug.

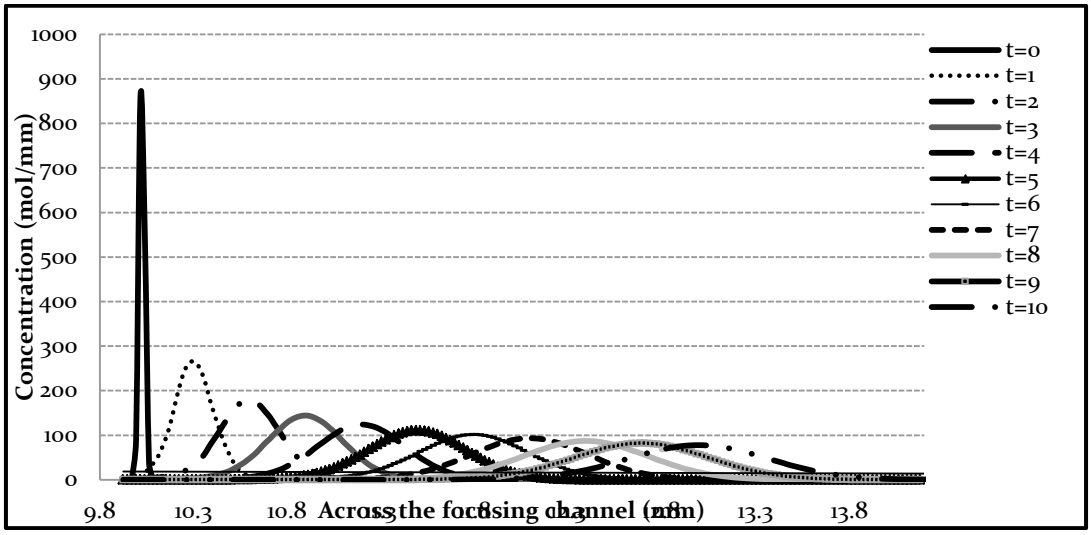

Figure 3-6: Finite element simulation results for the concentration profile along the horizontal channel at buffer velocity of 0.3mm/sec and pull back of -0.4mm/sec

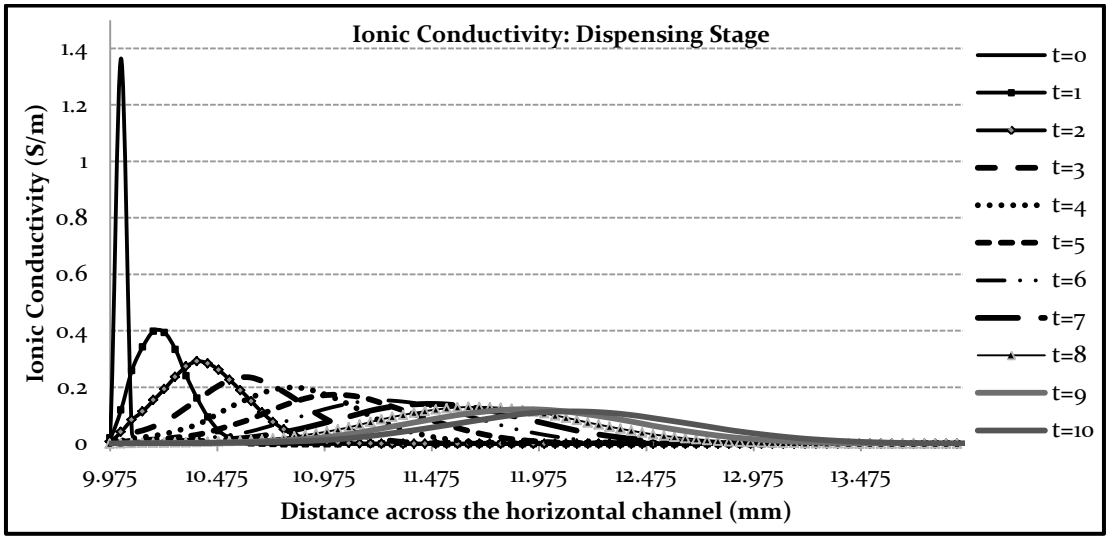

Figure 3-7: Ionic conductivity profile along the horizontal channel at buffer velocity=0.3mm/sec and pull back=-0.4mm/sec

3.2.3 Correlation of concentration of the injected plug with admittance

The concentration was measured as an integral at the boundary between the two pair of electrodes. The effect of the location of the electrodes with respect to the intersection was studied along with the relation between concentration and conductance profile. Figures 3-8 and 3-9 show the concentration and conductance profiles at electrodes placed at 200μm and 600 μm from the intersection. As expected, the results show that the conductance measured at 600 μm was lower than the conductance value at 200 μm, which corresponds to the diffusion of the plug as it travels. So, by fabricating the electrodes across the length of the channel the concentration profile can be compared by measuring the conductance on the array of electrodes as shown in the Figure 3-2.

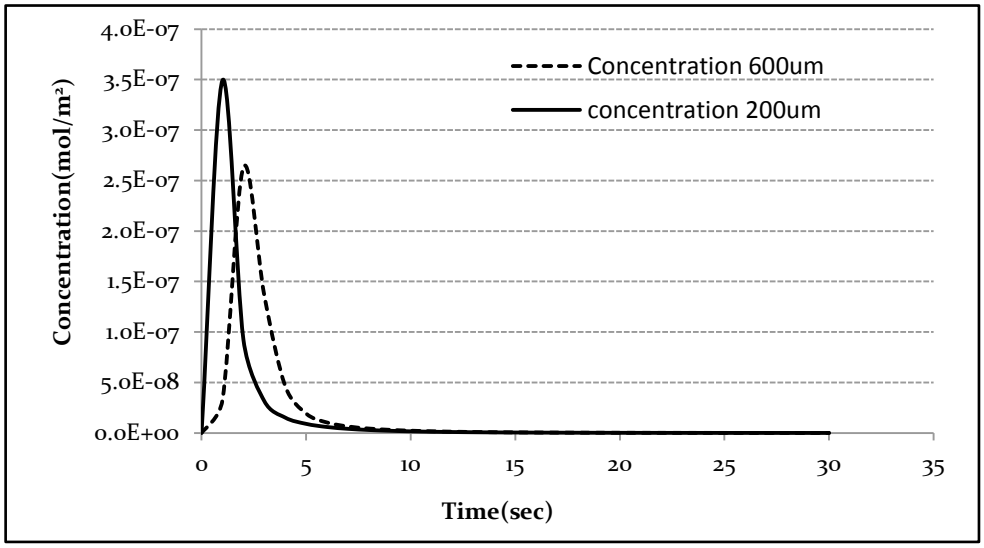

Figure 3-8: Concentration profile at 200 and 600um from the intersection (FEM)

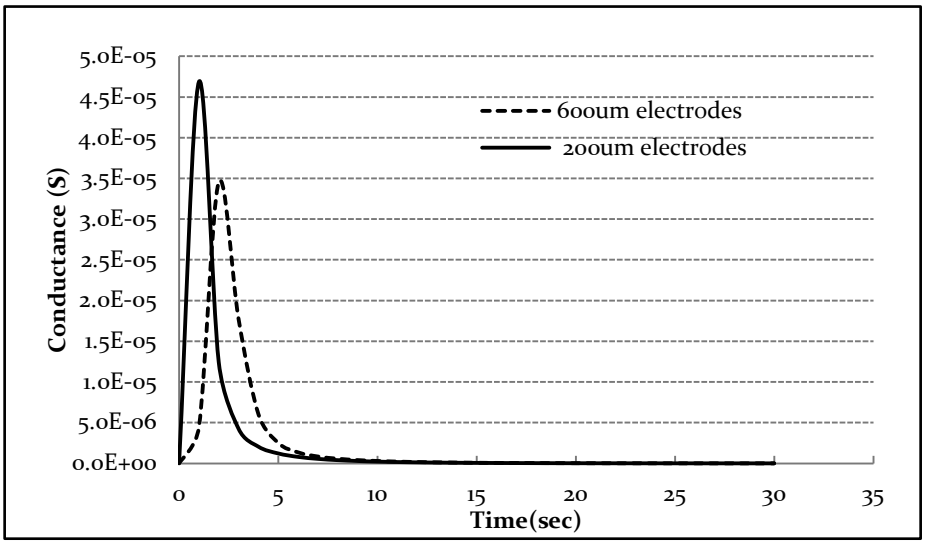

Figure 3-9: Comparison of conductance at 200 and 600um from the intersection (FEM)

3.2.4 Analysis of cell results

Figure 3-10 shows that the conductance measured between the two electrodes without a cell (with buffer only) is 2.1×10^{-10} S. The value of conductance was increased

by 2% if a live sample cell is placed between the electrodes at a height of 10µm from the electrodes. Further, if the cell dies the conductance measured between the electrodes is increased by almost 50% as compared to the conductance between electrodes with the live sample cell.

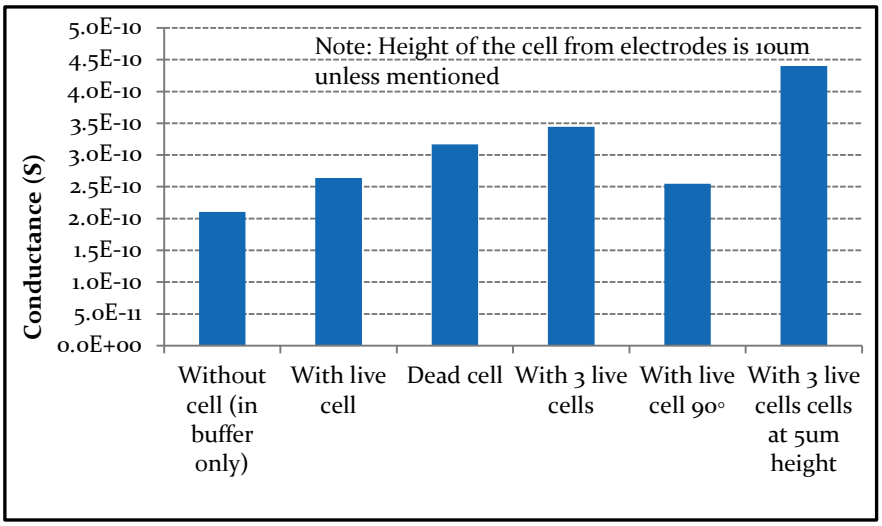

Figure 3-10: Comparison of measured conductance with different cell states

The effect of orientation was studied by positioning a cell at an angle of 0^o, 90^o with respect to the x-axis. Figure 3-11 shows the cell at angle of 90^o with respect to the x-axis. Figure 3-12 cell positioned at angle of 0^o. It is observed that the conductance decreased by 19% when the position of the cell is changed from 0^o to 90^o.

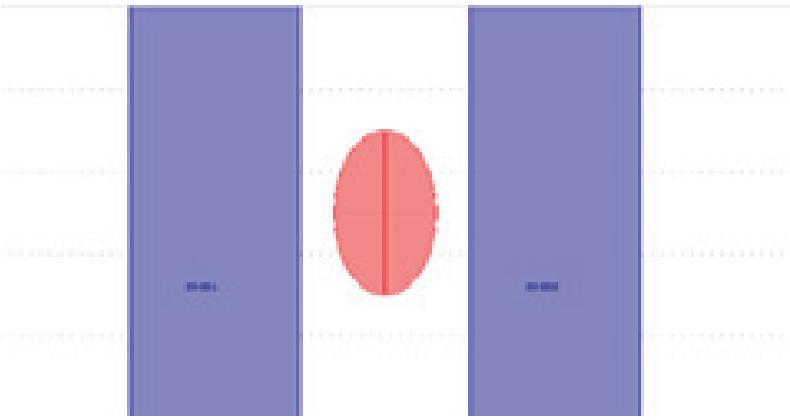

Figure 3-11: Placement of cell at 90 deg with respect to X-axis

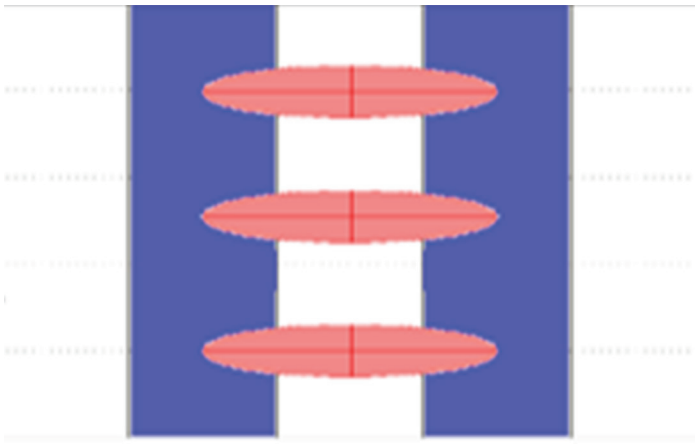

Figure 3-12: Array of three cells

3.2.4.1 Effect of concentration of cells

The effect of the concentration of cells on the impedance change was studied by increasing the number of cells from one to three. The cells are symmetrically placed with the existing cell to eliminate the effect of position on the impedance change. Figure 3-12 shows the X-Y plane view of the model with three cells. It was observed that the conductance increased by ~60% with the increase in cell concentration.

In order to study the effect of the distance of the cells from the plane of the electrodes, a layer of three cells was moved closer to the electrodes, at a height of 5μm. Figure 3-10 shows that the conductance increases by 28% when the layer of three cells is moved closer to the electrodes from 10μm to 5μm. This increase in conductance can be explained by Figure 3-13, where the height is due to the drop in the electric field gradient with distance from the plane of the electrode. It is expected that the maximum electric potential is near the electrodes an impedance change occurs when the layer of cells are placed on the surface of the electrode. As the distance of the cells increases from the plane of the electrodes the change in impedance decreases.

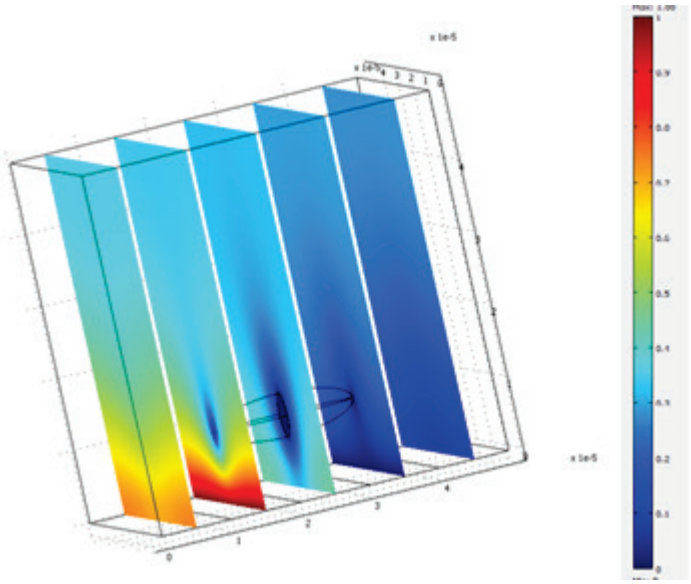

Figure 3-13: Electric potential distribution in the simulated model.

The change in the admittance with frequency 50Hz to 50MHz was also studied. It was observed that with the increase in the frequency, the susceptance value also increased. The conductance also increases. So, at higher frequencies the output signal will be smaller since admittance and impedance are inversely proportional. Figure 3-14 shows the effect of frequency on the admittance measured between the electrodes.

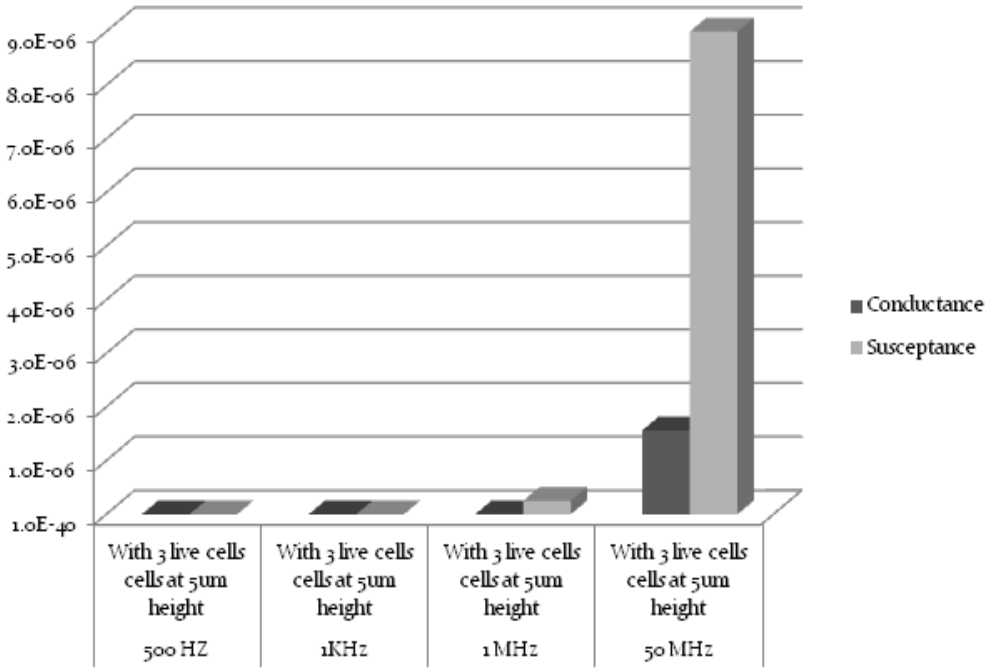

Figure 3-14: Effect of frequency on the admittance measured between the electrodes.

Figures 3-15 and Figure 3-16 concentration profiles and corresponding conductance values when drug is delivered to a cell are shown, respectively.

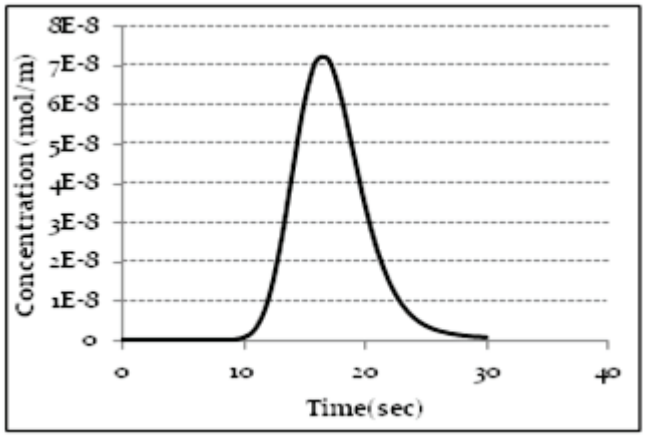

Figure 3-15: Concentration vs. Time (when drug is delivered to the cell chamber).

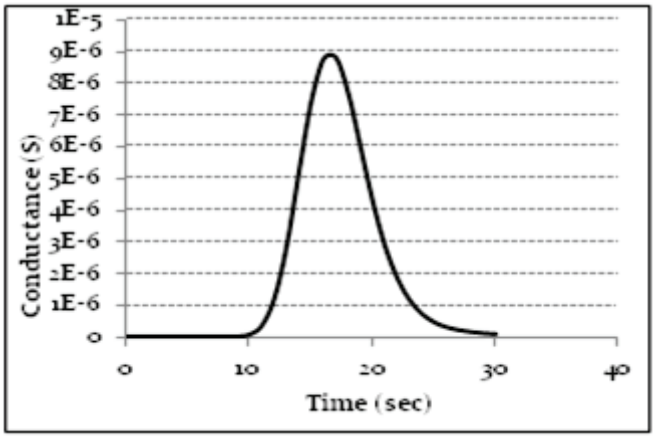

Figure 3-16: Conductance vs. Time (when drug is delivered to the cell chamber).

The results can be combined to get the final concentration and conductance correlation as shown in Figure 3-17. These graphs correspond to the real time scenario where a cell is trapped between the electrodes and a plug of a drug at some concentration is injected into the channel. The concentration of drug affects the metabolism of the cell resulting into a change in the corresponding conductance between the electrodes. The effect of concentration of drug can either improve the cell health or kill the cell; both these scenarios can be detected with the change in the conductance between the electrodes.

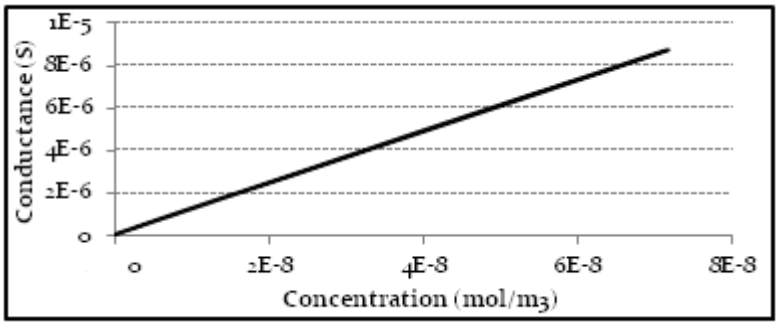

Figure 3-17: Concentration vs. Conductance (when drug is delivered to the cell chamber).

4. Accurate, real-time measurement of drug dosage

As explained in Chapter 1, before making the biosensor for pathogen detection a chemical sensor was designed, fabricated and tested for accurate measurement of varying drug dosage for real time analysis. Traditionally, dispensing of miscible liquids, for example a sample of drug and the carrier fluid flowing through a microfluidic channel, is experimentally determined using optical techniques [43]. Optical detection requires special labelling step, excitation source, and optics and detection circuitry, making the system requirements quite complex and expensive. We propose to use an electrical impedance technique to determine the concentration profile of a drug in a carrier fluid without any need for special labelling step. Concentration profile simulations as the drug plug moves along the microchannel have been performed and were explained in chapter 3. That data was used for design optimization to create drug-plug profiles of the desired shape. This detection method is inexpensive, straightforward and has the advantage that electrical signal can be conveniently processed and recorded, as compared to the conventional optical detection method [11]. The experimental set up can also be used in ECIS (Electric Cell-substrate Impedance Sensing) studies which measures the change in impedance of a small electrode to AC current flow. This includes cell culturing [12], cell counting [13] and pathogen detection [14] on a food sample.

This chapter reports designs, fabrication, packaging and testing of a highly sensitive technique for accurate and real-time measurement of minute variations in drug concentration. It also briefly discusses the fabrication and testing issues faced while developing this sensor.

There are many considerations that must be addressed while developing a microfluidic device with microelectrodes for monitoring the various electrical properties of the drug sample in real time for drug delivery and discovery applications. All the materials used must be biocompatible for at least relatively short period of time (weeks)

in order to carry out the experiments for the research. The need for spatially localized electrode sites in order to avoid misalignment issues must be balanced against parameters such as electrode impedance, and the signal-to-noise for performing accurate measurements.

4.1. Design

This section discusses the design of the first sensor utilized in this research to monitor varying drug concentration in real time environment. As discussed, electrical measurement technique is a label-free and less expensive alternative to fluorescence measurements [53]. Thereby, microelectrodes were designed to continuously monitor the change in electrical properties due to varying drug concentration in microchannel. Moreover, these electrodes provide low impedance electrical connection to the drug plug thereby, increasing the sensitivity of the sensor. Therefore, in this work arrays of microelectrodes were fabricated on a standard 3 × 3 inch glass slide using the standard lithography processes. Gold was chosen as the electrode material since it offers ease for measurement of biological. The polydimethylsiloxane (PDMS) microchannals were fabricated using soft lithography technique. Oxygen plasma activation technique was employed to bond the two individual components (Section 4.2.3).

4.1.1. Electrode

Our arrangement of electrodes avoids the potential electrode-channel misalignment issues [22].The array of electrode comprised of 8 electrode pairs with line width of 100μm. One electrode pair is shown on figure 4-1. Three variations with 40μm, 60μm and 100μm of inter-electrode gap were designed. Each end of the electrode pair had a square electrical pad (4 × 5 mm^2 ea.) to make electrical connections later. These arrays of electrodes were placed at the bottom of the microchannel.

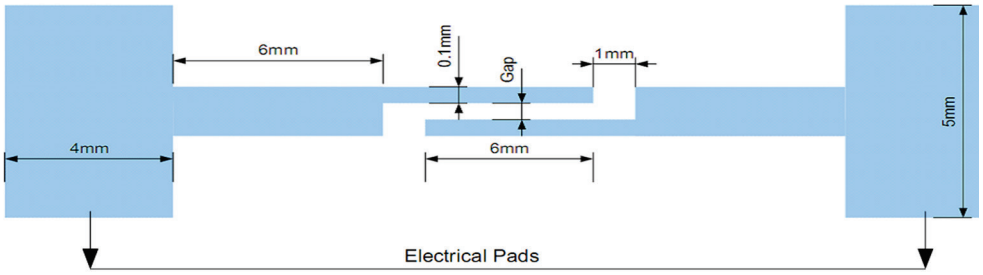

Figure 4-1: Design of an electrode pair for varying concentration profile measurement sensor

4.1.2. Micro-channel

In recent years, the development of micro-fluidic systems based on MEMS technologies has been attracting industrial as well as scientific attention. Early developments were mostly focussed on conventional semiconductor materials and techniques originally developed for the integrated circuit industry. The use of these materials and techniques is expensive due to extensive fabrication, packaging and testing. Recently, however, many alternative technologies using organic polymers have been reported. *Renaud et al* presented the use of Epon SU-8 photosensitive polymer for making multilayered channel networks [54]. Another polymer, polydimethylsiloxane (PDMS), is receiving an increasing amount of attention from the micro-fluidic fields. PDMS micro-molding techniques have been for microfluidic device fabrication [55, 56]. PDMS was utilized in this research for fabricating the microchannels.

Sylgard 184, a silicone elastomer kit obtained from Dow Corning Corporation (Midland, USA) was used in this research. The kit contains two chemicals: Base (part A) and Curing Agent (part B), that are mixed in 10:1 mass ratio. Both the chemicals are transparent, but quite viscous in nature. Mixing the two resin components produces a cross-linked network of dimethyl siloxane groups. PDMS is flexible so it can be easily removed from the master mold, leaving the master mold undamaged and ready to generate more devices.

Also, the PDMS substrate can be easily bonded to other PDMS, PMMA, and glass substrates using oxygen plasma [57] or corona discharge surface activation techniques [58].

The dimensions of the fabricated cross channel are as summarized in table 4-1.

Table 4-1: Dimensions of the fabricated micro cross-channel

	Width	Length
Loading Channel	**200 µm**	**1cm**
Dispensing Channel	**200 µm**	**3cm**

The microchannel was fabricated using an SU-8 mold. The reaction and waste reservoir were 4-mm in diameter. Before RIE bonding, holes were punched in the reaction and waste reservoir to make openings for the tubings. Figure 4-2 the design of the microchannel used in this sensor.

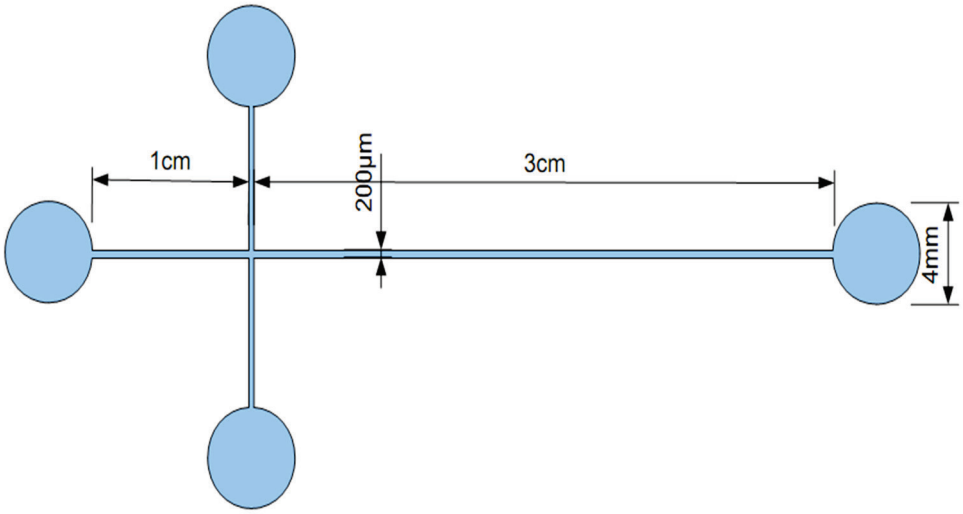

Figure 4-2: Design of the microchannel

The complete design of the sensor used for measuring varying drug concentration is as shown in Figure 4-3. The arrays of electrode were placed at the bottom of the microchannel.

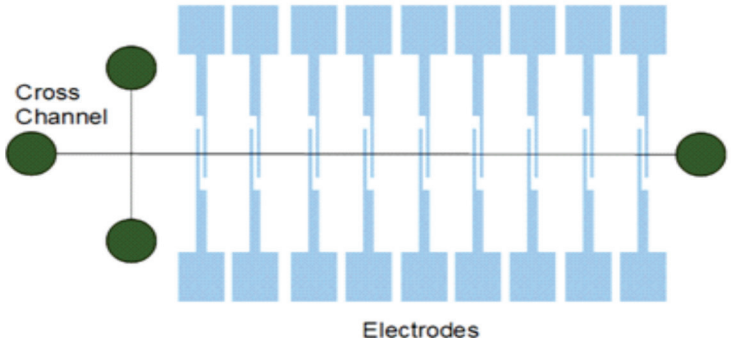

Figure 4-3: Design for varying concentration profile measurement sensor

4.2. Fabrication steps

4.2.1. Metal electrodes

Electrodes were fabricated using conventional photolithography process on glass slides. The glass slides of size 75 mm x 75 mm from Fisher Scientific Inc. were used for fabrication. Prior to fabrication, glass slides were RCA cleaned to get rid of any surface contamination followed by sputtering 100nm of Au (Gold) layer onto a 10nm of Cr (Chrome) layer. The layout of the design was drawn using designing software, Coventor. The design was then printed onto chrome mask from FineLine imaging, Colorado Springs, USA. This chrome mask was used for in contact photolithography in order to transfer the pattern onto the positive UV photoresist (1813). Electrodes patterns were transferred to the photoresist layer along with the pattern by exposing it using an aligner for 15 sec followed by 90sec of baking on a hot plate. The pattern was then developed in a developer solution for 60sec. The Au and Cr layers were etched in Au and Cr

etchants respectively. The choice of etchants depends on the minimum feature size of the pattern. If the minimum feature size is 20-100μm then standard TFA gold etchant and chrome etchant from Transene Company were used for etching. In case the minimum feature size was 2-10 μm then instead of TFA gold etchant, aqua regia (3 parts of hydrochloric acid and 1 part of nitric acid) was used for etching gold followed by diluted chrome etching(1 part of Cr etchant and 1 part of water). Finally, the photoresist layer was removed in an acetone bath. The Au electrodes fabrication process is illustrated in Figure 4-4.

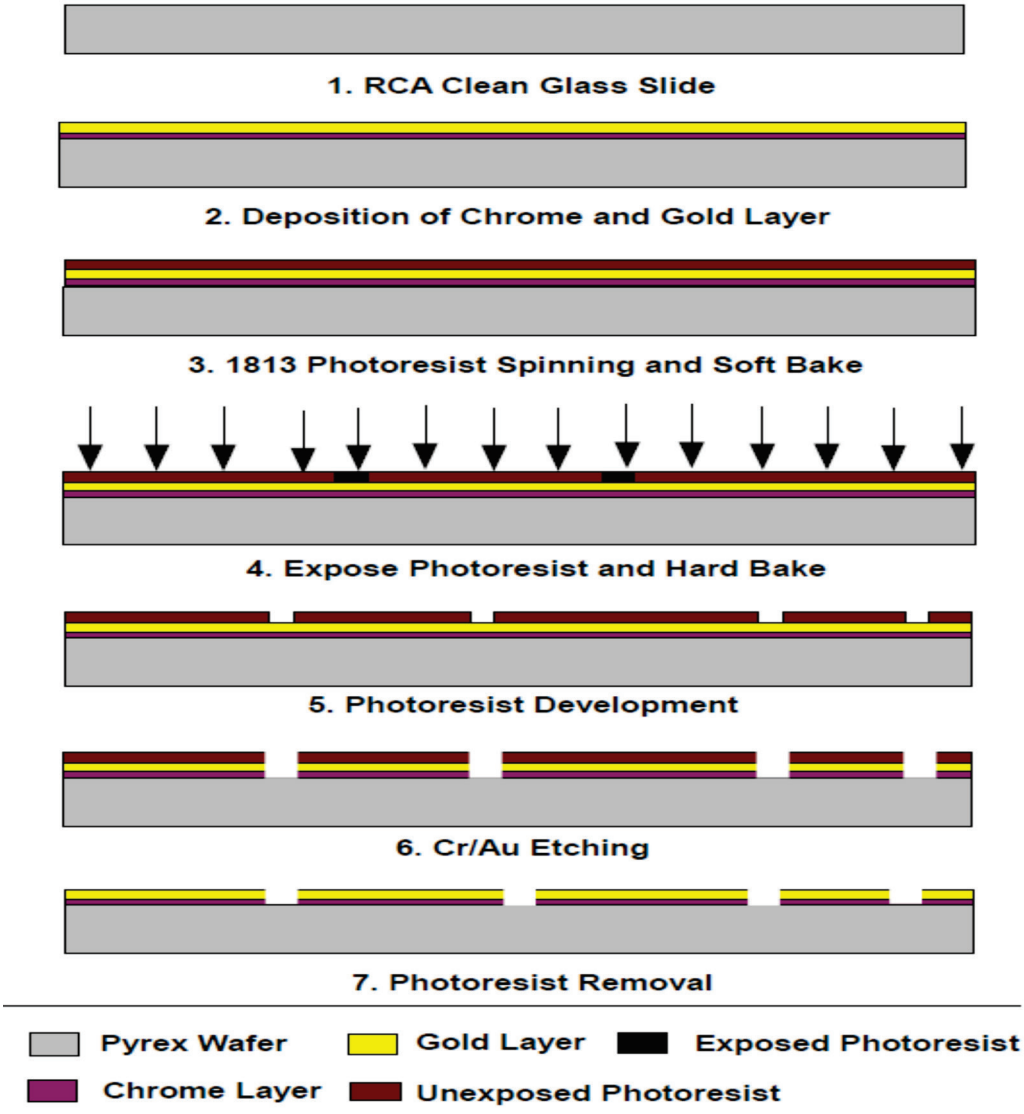

Figure 4-4: Microelectrodes fabrication flow process

One pair of the fabricated electrode is as shown in Figure 4-5.

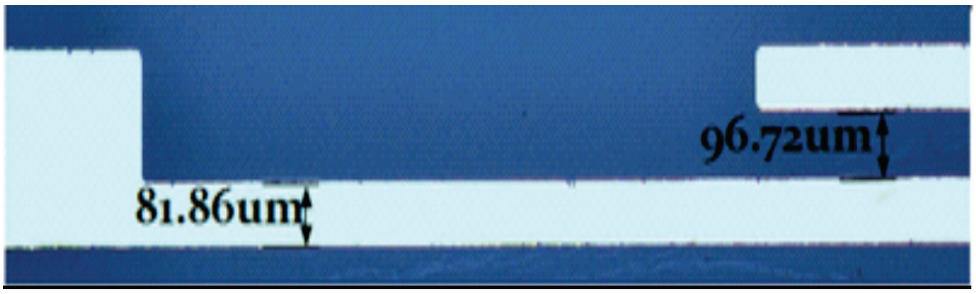

Figure 4-5: One pair of fabricated electrodes

4.2.2. Polydimethylsiloxane (PDMS) microchannels fabrication steps

A curing agent and PDMS prepolymer (SYLGARD 184 Silicone Elastomer Kit, Dow Corning, Midland, USA) were thoroughly mixed in a 1:10 weight ratio. The pre-polymer mixture was poured onto the master mold, and was degassed in a desiccator for 1 hour to remove any air bubbles in the mixture. The PDMS was cured for 5 hour at 80°C in a conventional oven. After curing, the PDMS replicas were peeled off from the master mold. Finally, the devices were cut to size (2 cm by 1cm) with a standard surgical steel blade, and the access holes were punched in the reservoirs using gauge 14 (0.069"-0.070") blunt needles (Zephyrtronics, Pomona, CA, USA). Figure 4-6 lists the process flow for fabricating PDMS microchannels.

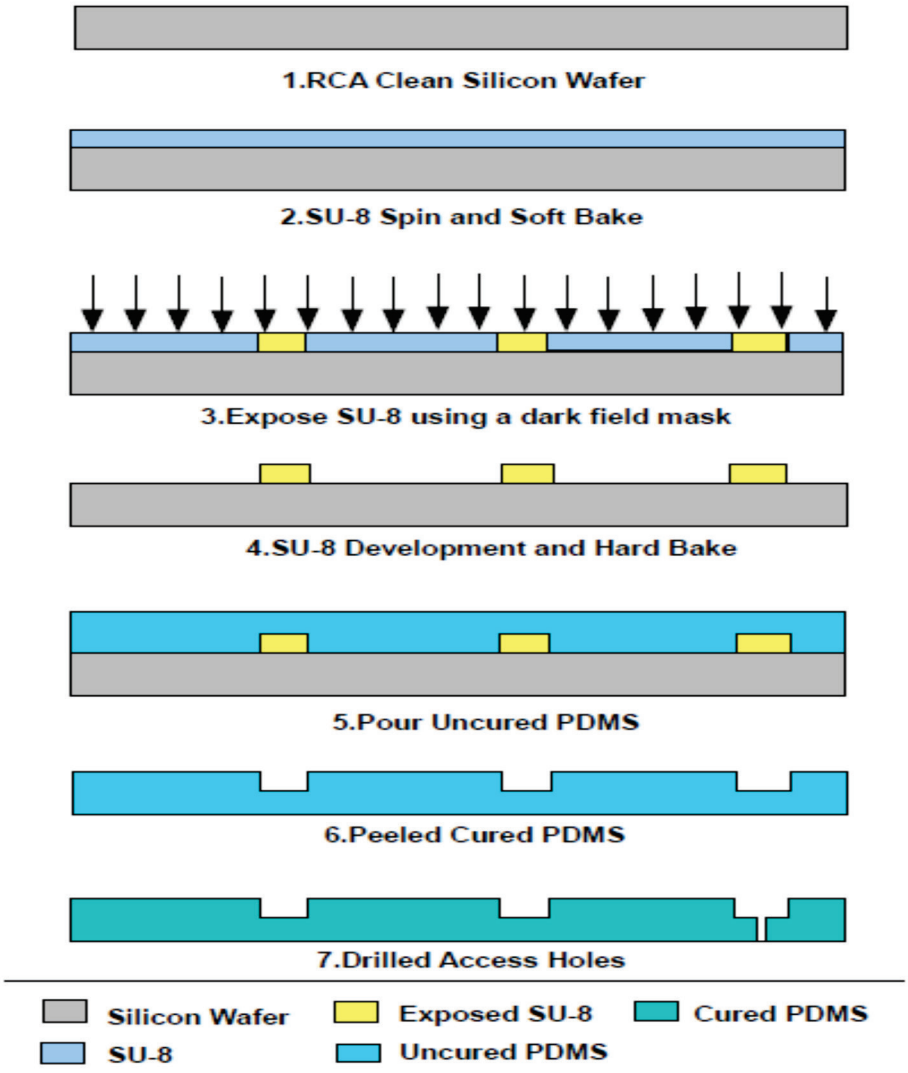

Figure 4-6: PDMS microchannels fabrication process flow

4.2.3. Bonding of individual components with reactive ion etching (RIE)

Oxygen plasma treatment for surface activation was carried out using a parallel-plate reactor reactive ion etching (RIE) system with both the samples placed on the water-cooled cathode. Experiments were performed to find optimum conditions of

plasma treatment by measuring the effects of three different process parameters: RF power, oxygen partial pressure, and treatment time. It was found that optimal process parameters for activating the surfaces for bonding were 70W of RF forward power, 75 mTorr of oxygen pressure and 10 sec of treatment time. Plasma-treated electrode patterned glass slide and PDMS microchannel were immediately bonded with activated surfaces facing each other. At this point, no external forces were applied on the samples to assist the bonding procedure. After 5 min, the bonded area was quantified via manual examination (pulling the pieces apart to determine the percent area bonded). Figure 4-7 shows the fabricated microfluidic chip with electrodes placed at the bottom of the microchannel bonded using oxygen plasma treatment with access holes and tubing attached.

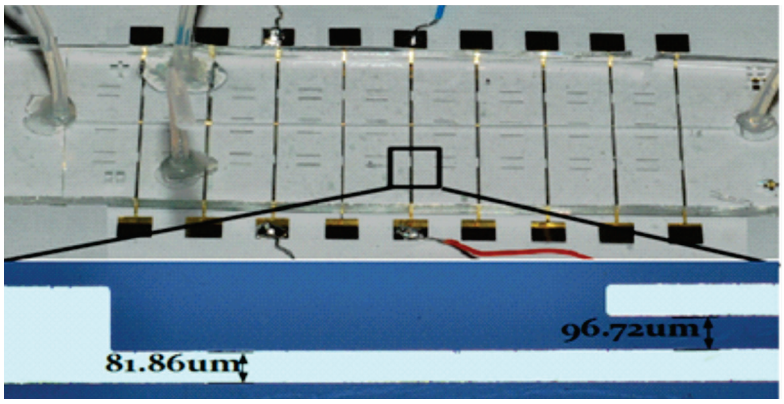

Figure 4-7: Fabricated microfluidic chip

4.3. Experimental results

This section specifies the reagents used for experimentation, describes the experimental set up and discusses the results for the first microfluidic sensor utilized in the research.

4.3.1. Preparation of reagents

For initial set of experiments, varying molar concentrations of sodium (Na^+) ion solution ranging from 10pMol/ml to 1 Mol/ml was used. For this 1 Mol/ml sodium chloride

(NaCl) was obtained from Ravinder Reddy in chemistry department, Simon Fraser University. This was subsequently diluted to prepare further dilutions of NaCl solution. Since calcium (Ca^{2+}) ions are the main target of this research, final experimental results were done using for various molar concentrations of calcium chloride ($CaCl_2$) solution ions ranging from 10pMol/ml to 1 Mol/ml. The choice for Ca^{2+} ions was made since they are more realistic for drug development studies for cardiovascular diseases.

4.3.2. Experimental set up and results

A lock-in amplifier (HF2LI by Zurich Instruments) as shown in Figure 4-8 was used to generate the stimulation signal. The main advantage of using lock-in amplifier is that it is capable of accurate measurement of signal levels with controllable levels of noise through adjustment of measurement bandwidth. Even when noise and signal are indistinguishable in the time domain, if the signal has a definite frequency band and there is no large interference or noise peak within that band, noise and signal can be separated sufficiently in the frequency domain using a lock-in amplifier. The variable gain input stage pre-processes the signal by amplifying it to a level suitable for the demodulator which multiply two waveforms together and remove noise by passing the output through a low pass filter.

Figure 4-8: Lock-in amplifier used for experimental results

The experimental setup is schematically shown in Figure 4-9.

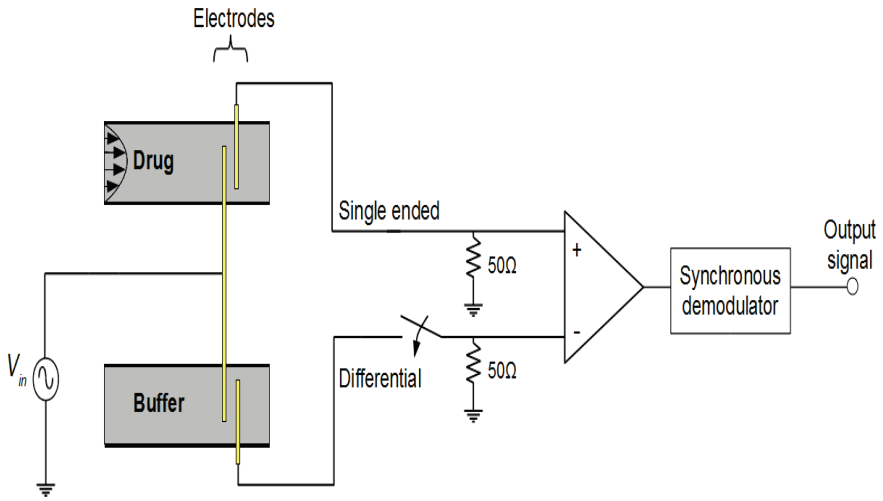

Figure 4-9: Experimental setup for single-ended and differential measurements

An array of electrodes were employed to continuously monitor the electrical properties of the fluid in microchannels to estimate the profile of a drug plug as it moves along a microchannel while it diffuses into the buffer solution. Initial set of experiments comprised of real time analysis of the output signal for varying drug concentration. Figure 4-10 illustrates experimentally acquired output signal profile for two different drug concentrations (Na^+ ions) at the intersection of the microchannel over time. It can be observed that the rate of change of output signal is dependent on the rate of change of concentration of the sample drug as obtained from finite element analysis.

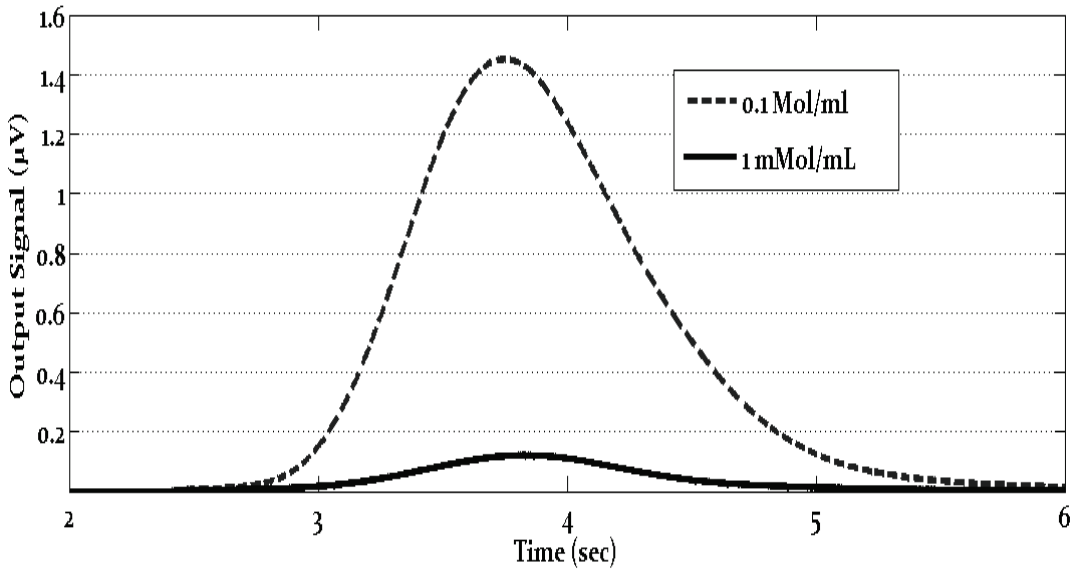

Figure 4-10: Real time experimental results for output signal for 0.1Mol/ml and 1mMol/mL concentration of Na^+ ions.

Following this, in the first set of experiments, real time measurements were recorded by exciting one electrode with a sinusoidal voltage and measuring the conduction current (converted to a voltage through a 50Ω resistor) for various concentrations of drug (Ca^{2+} ions). However, for low drug concentrations, majority of conduction current is through the buffer which deteriorates the measurement accuracy. To circumvent this problem, real time differential measurements were taken across two sets of electrodes where the additional set of electrodes was kept in the buffer solution.

The characteristic transient curves for single ended and differential measurements for various drug concentrations are compared in Figure 4-11. The signal amplitude varied linearly with drug concentration. It can be seen that by rejecting the common-mode signals, the dynamic range of concentration measurements is increased considerably, enabling us to measure drug concentration down to less than10pMol/mL. Thereby, the sensitivity of the chip is considerably increased.

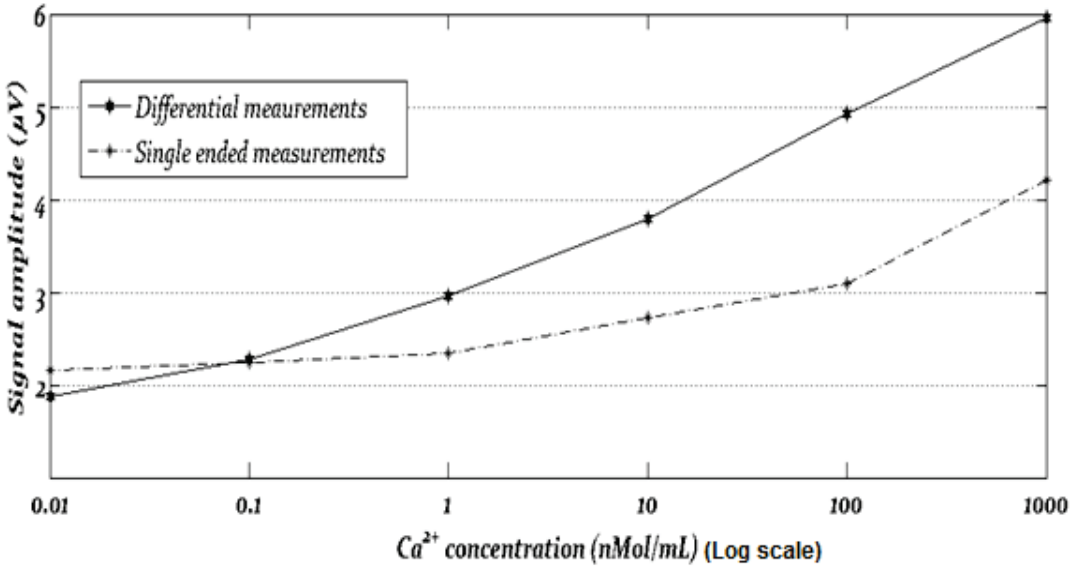

Figure 4-11: Comparison of single-ended and differential real time measurements for various concentrations of Ca^{2+} ions

4.3.3. Challenges

Since very minute concentrations of the drug were used, it was essential to the thoroughly clean the microchannel to eliminate any moisture. This was done by flushing the microchannel with deionised (DI) water followed by degassing the microfluidic chip by placing it in the vacuum oven for 15-20 minutes. Degassing also decreased the formation of bubbles in the microchannel which hindered in the formation of plug. The presence if bubbles in the channel caused hindrance in the formation of the plug, thereby, the whole experiment set up was to be repeated again.

5. Biosensor for pathogen detection

The concern for food safety and quality has been a major area of concern for decades. Nevertheless, the likelihood of contaminated food has increased by foodborne pathogens and toxins. Many pathogenic microorganisms in food can lead to severe health consequences in animals and humans. Therefore, early and timely detection of these pathogens is one of the key areas of research

This chapter outlines the biosensor utilized in this research used to detect the presence of bacterial colonies in a given food sample. Biosensor
based process is robust and is an effective pathogen detection technique. Among the various types of biosensor, electrical biosensor offers a more reliable and time efficient detection method since it overcomes human errors. This detection set up enables us to count the number of bacterial colonies while they are being cultured irrespective of the type of bacteria used. Therefore, it was not necessary to label the bacteria. As shown later in this chapter, the design of the pathogen detection biosensor consists mainly of an array of interdigitated electrodes suitably modified with a biological receptor, so that when the process of interest takes place, an impedance change can be observed.

5.1. Design

This section discusses the design of the biosensor utilized in this research, to detect pathogens such as E-Coli incubated on the surface of an agar medium. For all electrical based biosensor applications, monitoring the potentials and electrical impedance requires a cell culture substrate. This substrate contains microelectrodes upon which the cells can be cultured. Moreover, the electrode must provide a low impedance electrical connection to the cell. The adhesion of cells to the passive layer is also of considerable importance as the loosely coupled cell provides a shunt path for current. This thereby decreases the signal strength for both impedance and action potential measurements.

For this work, 2 × 3 inch glass substrates were utilized to pattern the microelectrodes while the cell chamber was fabricated using PDMS. Similar to the first sensor, gold was chosen to fabricate electrodes since it can be easily used for measuring biological signals.

5.1.1. Interdigitated array of electrodes

This section describes the design used for patterning the microelectrodes for pathogen detection biosensor. The array of electrodes comprised of 14 pairs of interdigitated electrodes with length of 2.5 cm, width of 100 µm and inter-electrode gap of 100 µm. This gap size was chosen so that the presence of bacterial colonies could be detected. If the gap size is too small then the electrodes will measure almost the same, further deteriorating the detection process. Also this width of the electrodes was chosen so that it is comparable to the thickness of the agar film deposited on the top the electrodes which would also hamper the measurement quality. Electrode design used in this research is shown in Figure 5-1. One end of each electrode had an electrical pad of size 2 × 2 mm^2 to make the electrical connections later

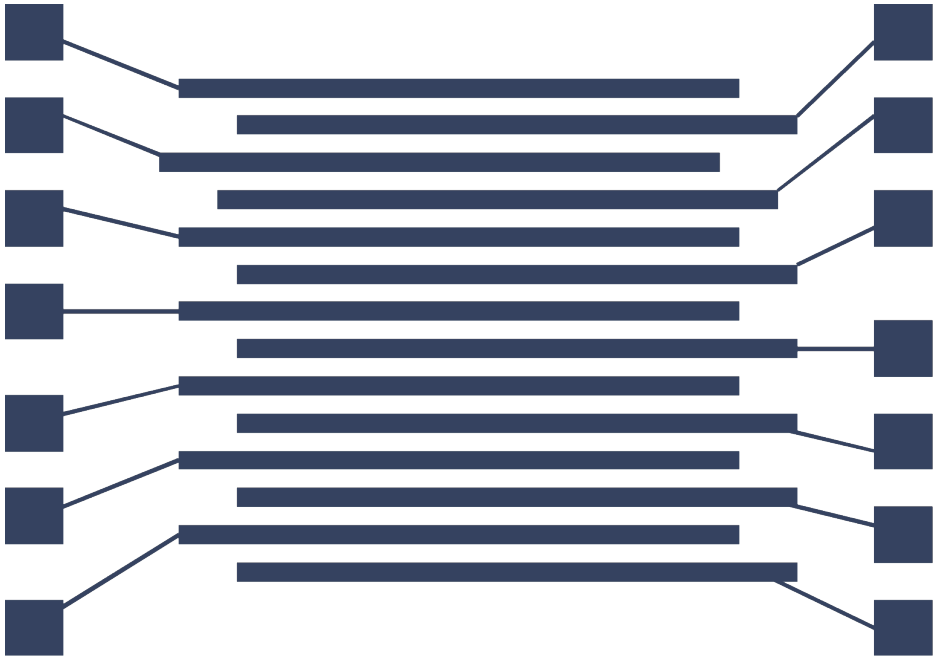

Figure 5-1: Design for the electrodes used for pathogen detection

5.1.2. Microchamber

A PDMS chamber was designed in such a way that it formed a boundary wall around the entire electrode area. The thickness or height of these chambers was 1mm. The mold used to make the chamber was prepared by gluing a 1 × 3 inch glass slide on a 4 inch silicon wafer using Loctite superglue. Freshly prepared agar medium was poured on this microchamber such that the microelectrodes are at the bottom of the agar medium. Once the agar medium is cooled it transforms into a jelly state. E-Coli (DH5α) are cultured on the top of this agar layer inside an over calibrated at a temperature of 37°C.

5.2. Fabrication steps

As discussed in chapter 4, the microelectrodes were fabricated through the process steps mentioned in section 4.2.1. Since the electrodes had inter-gap of 100μm instead of standard TFA gold etchant from Transene Company, Inc., aqua regia (3 parts of HCl and 1 part of HNO_3) was used for etching gold followed by diluted chrome etching. Etching with standard TFA gold etchant peeled off of the electrodes form the glass substrate due to deep undercuts. Microchamber, used to culture the bacteria was fabricated out of PDMS as explained in section 4.2.2.

The complete fabricated pathogen detection biosensor is as shown in Figure 5-2.

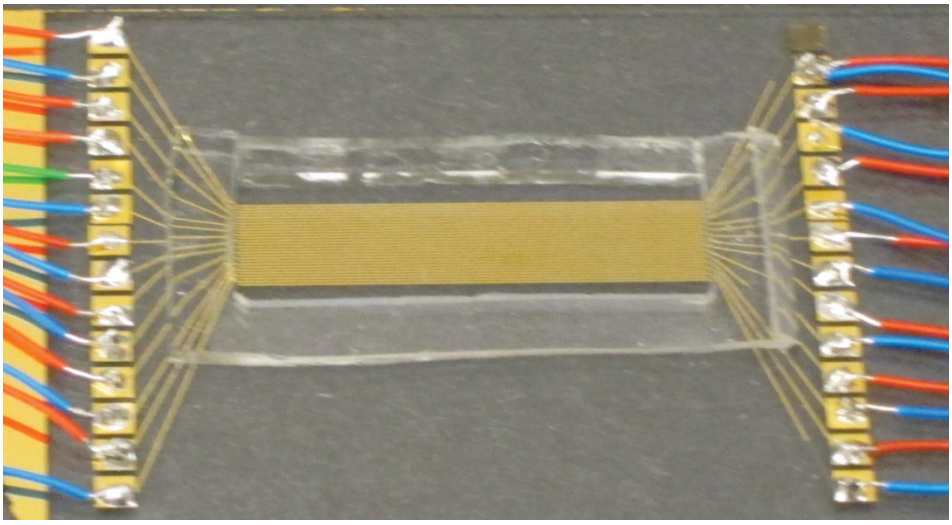

Figure 5-2 : Fabricated biosensor with the PDMS chamber

5.3. Experimental results

This section discusses the preparation of reagents, the experimental set up and results for pathogen detection biosensor developed in the research.

5.3.1. Preparation of reagents

5.3.1.1. LB Agar medium

120mL of LB agar medium was prepared in Dr Beischlag's Laboratory in Faculty of Health Sciences. 3 capsules of LB medium from MPBiomedical, 1.8 grams of agar (powder) from Anachemia were added to an autoclaved flask containing 120ml of deionised (DI) water. The mixture was thoroughly mixed before placing it for autoclaving. The autoclaving step takes about 55 minutes.

5.3.1.2. Preparation of cells

DH5α E-Coli bacteria were used to prepare the plate for culturing since it's a non-pathogenic to normal healthy individuals. An already prepared streak of culture plate was used to find the correct dilution of cells to form single colonies on the agar plate. A single colony was transferred from this plate using a tooth pick into a test tube containing 10 ml of 0.1% peptone water. The tooth pick was manually swirled in order to mix the cells in the solution. This was labelled as tube#1. Series of dilutions were done

and it was found that third dilution, tube#3 produced single colonies (as shown in Figure 5-3) as required. The cell solution prepared could be used for up to a week by storing them at 4°C.

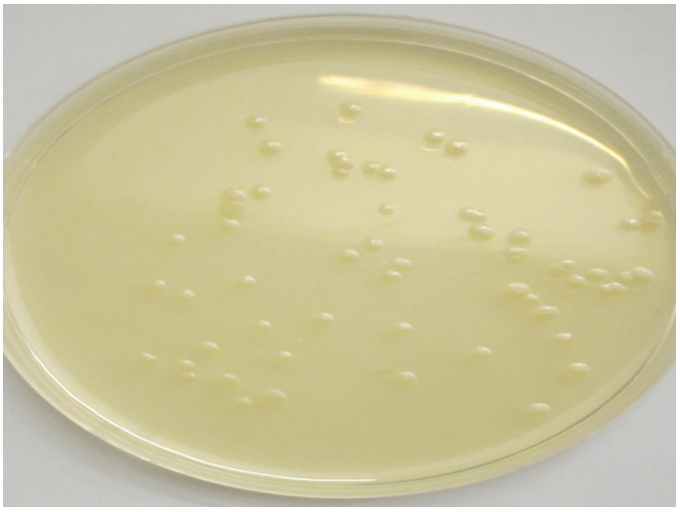

Figure 5-3: Visible E-Coli colonies after 24 hours of incubation

5.3.1.3. Culture chamber

In order to culture the bacteria on the top of the agar layer placed on the surface of interdigitated electrodes, a PDMS chamber was designed. The agar media prepared was heated in the microwave until it liquefied, and then cooled down to 55°C in a bath tub. This liquefied agar was poured on to the chamber using a pipette so that it covers the entire microchamber uniformly. It was left undisturbed until it solidifies. After it solidifies, 400µL of cell solution was dropped at the center of the chamber using pipette and evenly spread using an autoclaved cell spreading rod. The chamber prepared is as shown in Figure 5-4. Allow the cell solution on top of the agar film to dry for about 15 to 20 minutes at room temperature, before placing it inside the oven at 37°C for culturing.

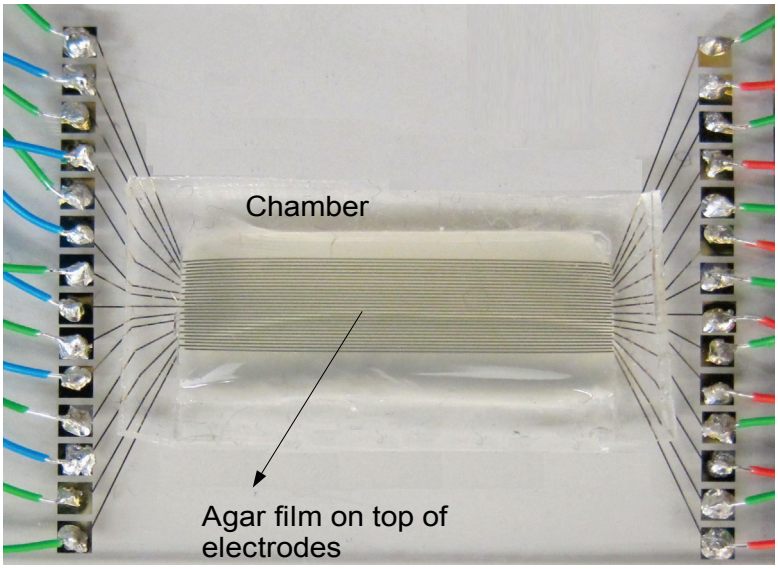

Figure 5-4 : Fabricated biosensor chip with agar film on top for culturing bacteria

5.3.2. Experimental set up

The experimental setup for pathogen detection comprised of four major components, namely, the mesh with pathogen sample, the computer workstation, the lock-in amplifier and the switching circuit as shown in Figure 5-5. While the first three were consistent with previous experiments, a switching circuit was added to release an automated measurement process with respect to multiple electrode pairs under test. This switching circuit was contributed by Tim Tan.

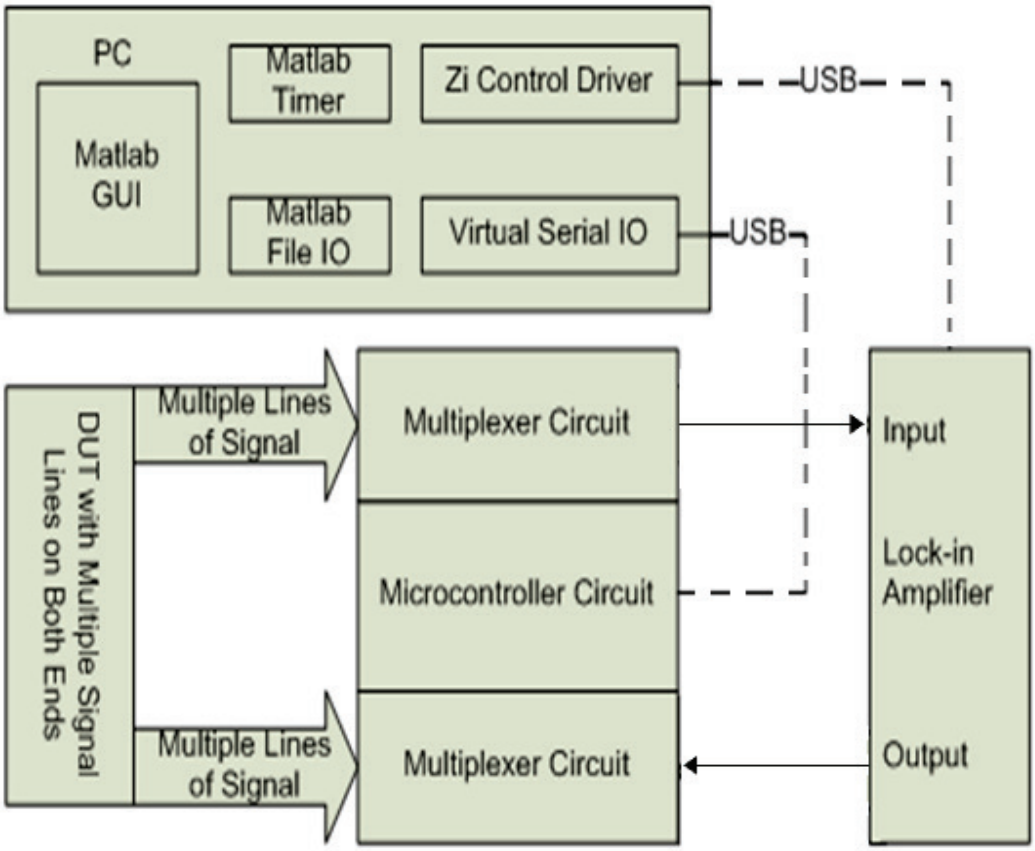

Figure 5-5 : Block diagram for experimental set up for pathogen detection biosensor

The major characteristic of the device under test in this experiment is that it is a passive device with multiple electrodes on both ends. Meanwhile, the objective of the test setup was to measure the impedance between two pairs of electrodes in an automatic manner. The lock-in amplifier was used to perform the measurement between two given terminals, while the circuit tree between the lock-in amplifier and the device under test connects the lock-in amplifier terminals to the intended electrodes. As shown

in figure 5-5, two multiplexer circuits were built for the job. A personal computer was used to communicate with a microcontroller. The main function of the microcontroller was to control switching of multiplexer circuits, collect data from the lock-in amplifier and write them to the local hard drive. The software setup used in the workstation features Matlab to handle timer, file IO (Input/Output), serial communication, data polling from the lock-in amplifier and user interfacing. The experimental set up is as shown in Figure 5-6.

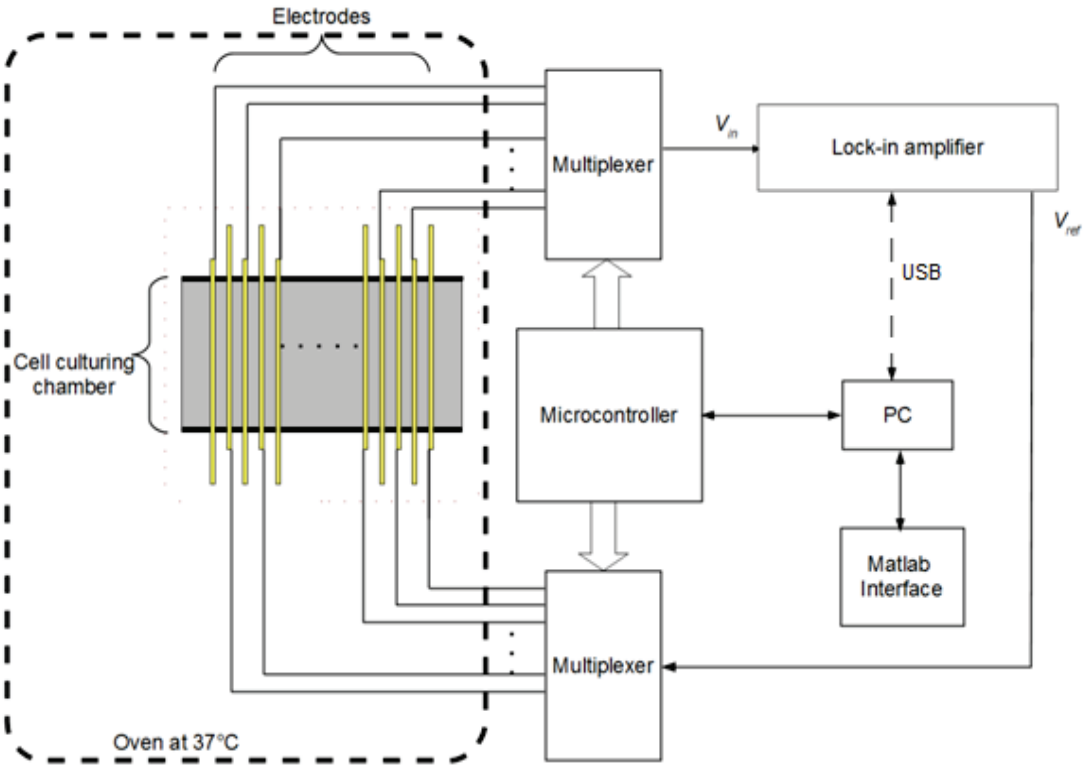

Figure 5-6: Experimental set up for pathogen detection biosensor

The actual experimental set up comprising of a computer, lock-in amplifier, PCB and an oven calibrated at 37°C is as shown in Figure 5-7. This oven was used to culture the bacteria over the electrodes and a thermometer was attached at the top of the oven, to monitor the temperature. The pathogen detection biosensor was placed inside a petri dish along with damped wipes to maintain the moisture. This was to ensure that the thin agar layer on top of the electrodes does not evaporate due to heat.

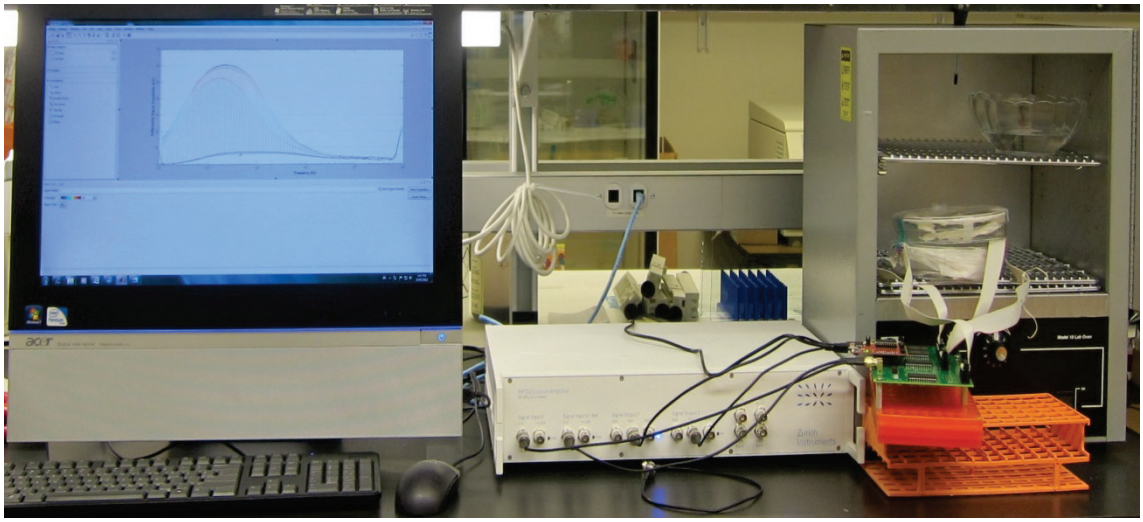

Figure 5-7: Experimental set-up used in the research

As shown in the enlarged picture in Figure 5-8, a bowl of water inside the oven was kept to maintain the humidity inside the oven.

Figure 5-8: Oven used as an incubator to culture bacteria showing a water bowl to maintain humidity

5.3.2.1. The MC-MUX (Microcontroller-Multiplexer) circuit

Two multiplexer circuits (sometime only one was desired) and the microcontroller circuit were built together. They were built on bread boards at the beginning and moved to a printed circuit board (PCB) later.

The microcontroller used was MSP420G2452 (20DIP), which had two pins for serial communication, four pins for debugging, V_{dd}, ground terminal and twelve available GPIOs (General Purpose Input/Outputs). Each six GPIOs were used to control one multiplexer circuit, which enables 64 × 1 multiplexing capability. The choice of multiplexer was 74HC4067N (24DIP), which delivered 16 to 1 multiplexing. With the help of an additional 8 to 1 multiplexer, 74HC4051N (16DIP), and four resisters, used for disabling and four multiplexers forming a 64 to 1 multiplexing unit. Two of those units were printed in the final PCB. The PCB also had some auxiliary utilities for ease of experiments.

The microcontroller from TI (Texas Instruments) LaunchPad board was used to enable communication with personal computer workstation via USB (Universal serial board). The LaunchPad board was bridged to the designed PCB. Once the Code Composer Studio driver was installed on the workstation, the microcontroller could be used as a serial device. The microcontroller was programmed to receive discrete bytes of signal and reply with a byte count for the host to verify the integrity of the communication. After receiving every two bytes, the microcontroller applies the first byte to the 6 GPIOs on port 1 and the second on port 2 to modify the state of multiplexers.

There were a few history revisions of this circuit and the most appropriate one was adopted in the PCB. History circuits include one with all 8×1 multiplexers connecting multiple electrodes at the same time. The microcontroller software was also improved over time. Figure 5-9 shows the PCB used in this research. The left side four multiplexers are used to give input signal, whereas the output signal was measured for the four multiplexers on the right side of the board. For this research, only two (each) multiplexers were utilized.

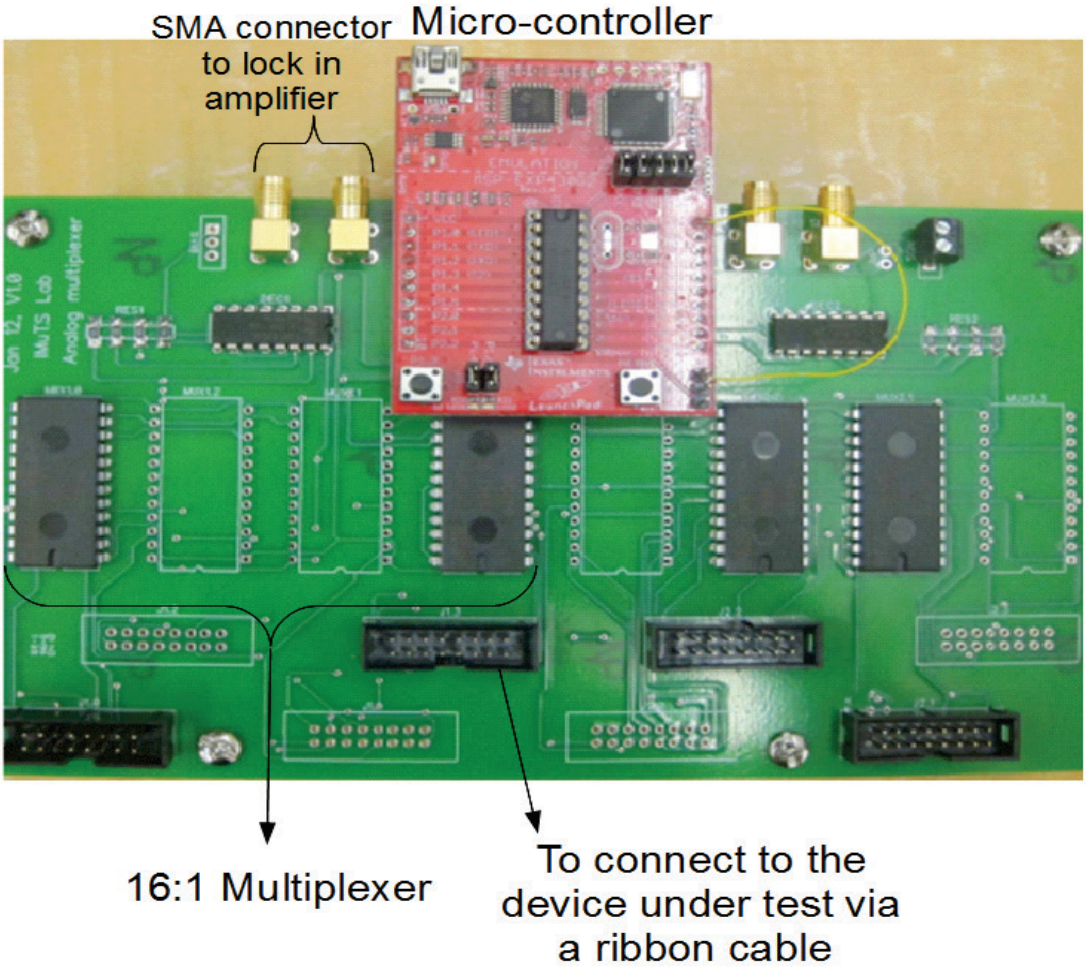

Figure 5-9: Printed circuit board for microcontroller-multiplexer circuit

5.3.2.2. The Matlab Software Suite

Matlab was used extensively in the setup of this experiment that comprised of namely the following:

- Timer to trigger the experiment in automated experiments
- Driver for the lock-in amplifier to read data from lock-in amplifier and apply various settings
- Saving data

- Serial communication with microcontroller and its integrity check (required Code Composer Studio drivers)
- Graphical User Interface(GUI) as illustrated in Figure 5-10 to enable and coordinate above functions as well as user interfacing

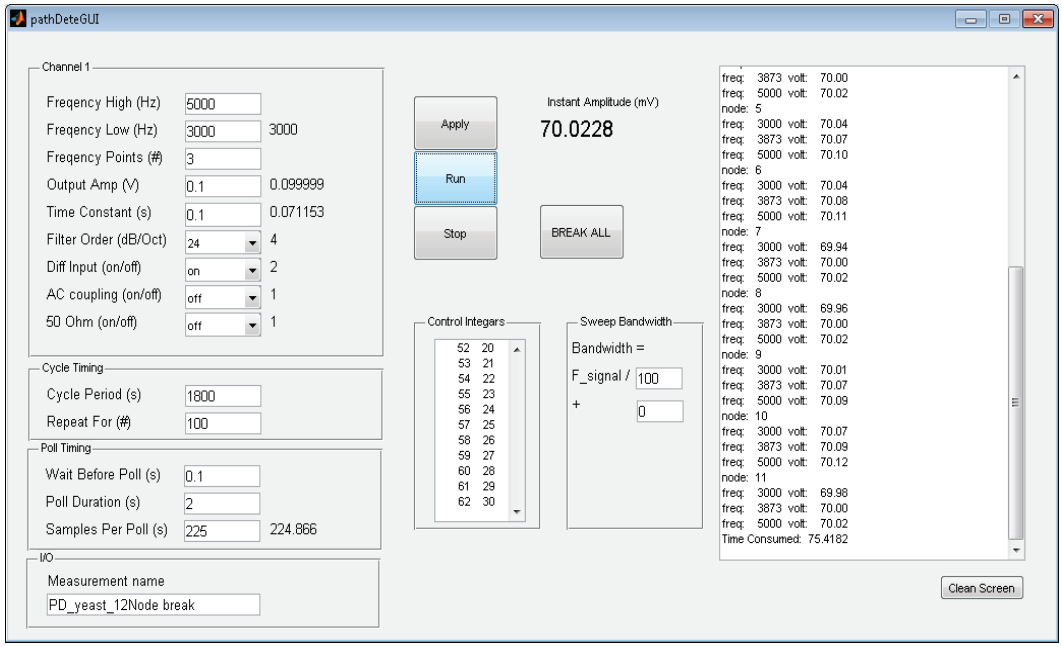

Figure 5-10: Comprehensive matlab graphical user interface

The default software provided by Zurich Instruments, ziControl, is already capable of data saving and setting various configurations, but it does not meet our requirements when a coordinated switching was desired or when flexible data saving was to be automated timely. In order to be consistent with the lock-in-amplifier GUI, the Matlab Software Suite resembled the look and feel of ziControl with additional features for timer and data saving. A message window was used to printout necessary messages. Other scripts independent of the GUI were also written to plot the acquired data for analysis.

5.3.3. Results with yeast bacteria

As discussed before, an array of interdigitated electrodes was employed to monitor the electrical properties of the bacteria cultured over the electrodes on top of agar film. For this, switching circuit was used to frequently monitor the signal over each pair of electrode. The initial experiments were carried out to test the sensitivity of the electrical biosensor. This was done by culturing yeast cells suspended in sugar water at room temperature. Yeast cells normally incubate at room temperature after 4 minutes. Signal amplitude was found to increase on electrodes where yeast cell cultured. Signal amplitude for three sets of frequencies 1 kHz, 2.2 kHz and 5 kHz was measured across electrode 2, 3 and 13. As shown in Figure 5-11, Figure 5-12 and Figure 5-13 there was an increase of 3 mV, 4.5 mV and 5 mV in amplitude across electrode pair #2 and #3 and #4, respectively and no change across electrode pair #13, since there was yeast growth across electrode pair #2, #3 and #4 and none across electrode pair #13, as shown in Figure 5-14.

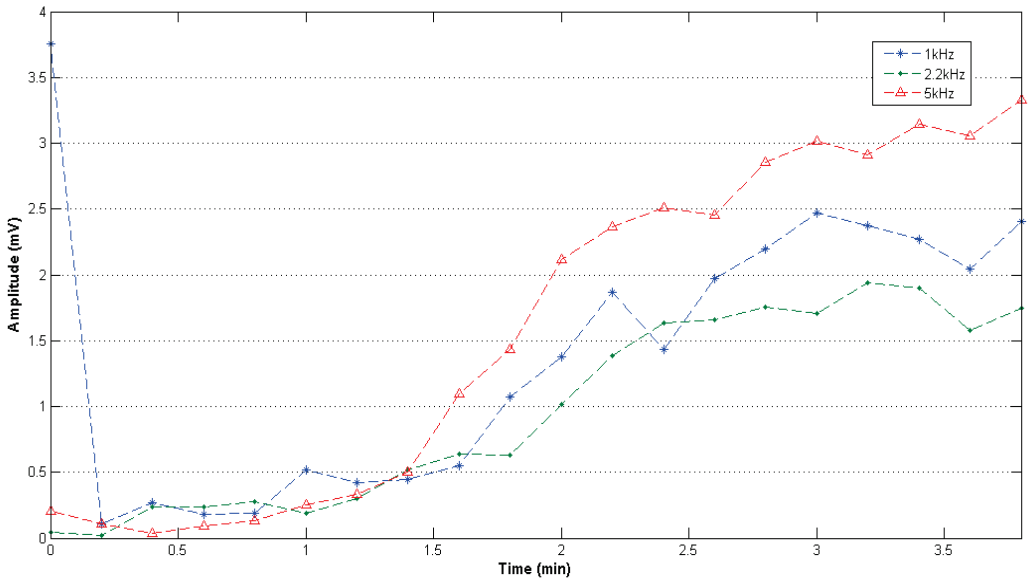

Figure 5-11: Signal amplitude variation over time across electrode pair #2

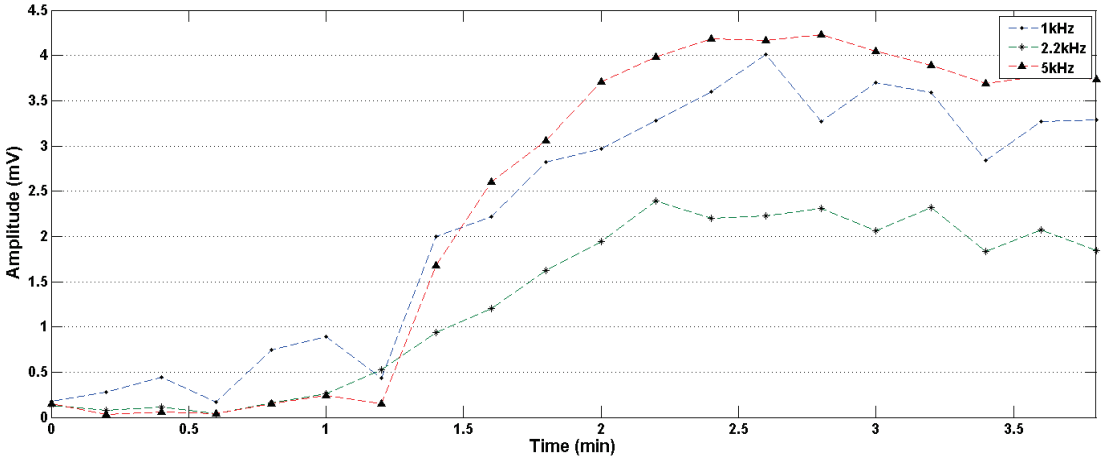

Figure 5-12: Signal amplitude variation over time across electrode pair #3

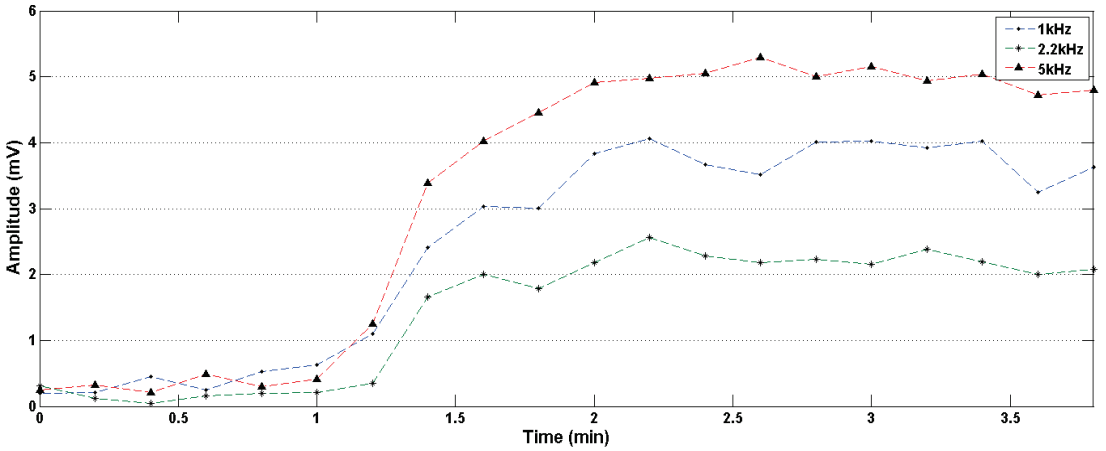

Figure 5-13: Signal amplitude variation over time across electrode pair #4

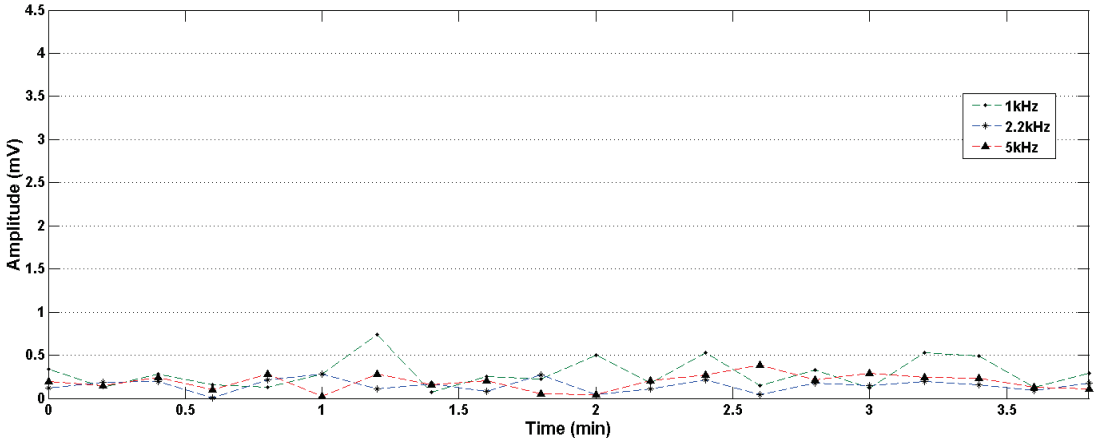

Figure 5-14 : Signal amplitude variation over time across electrode pair #13

The contour plot as shown in Figure 5-15 clearly indicates a significant signal increase across electrodes where yeast was cultured as compared to those electrodes where no yeast lived. It can be seen that was no change in impedance at rest of electrodes pairs where no yeast cell was present.

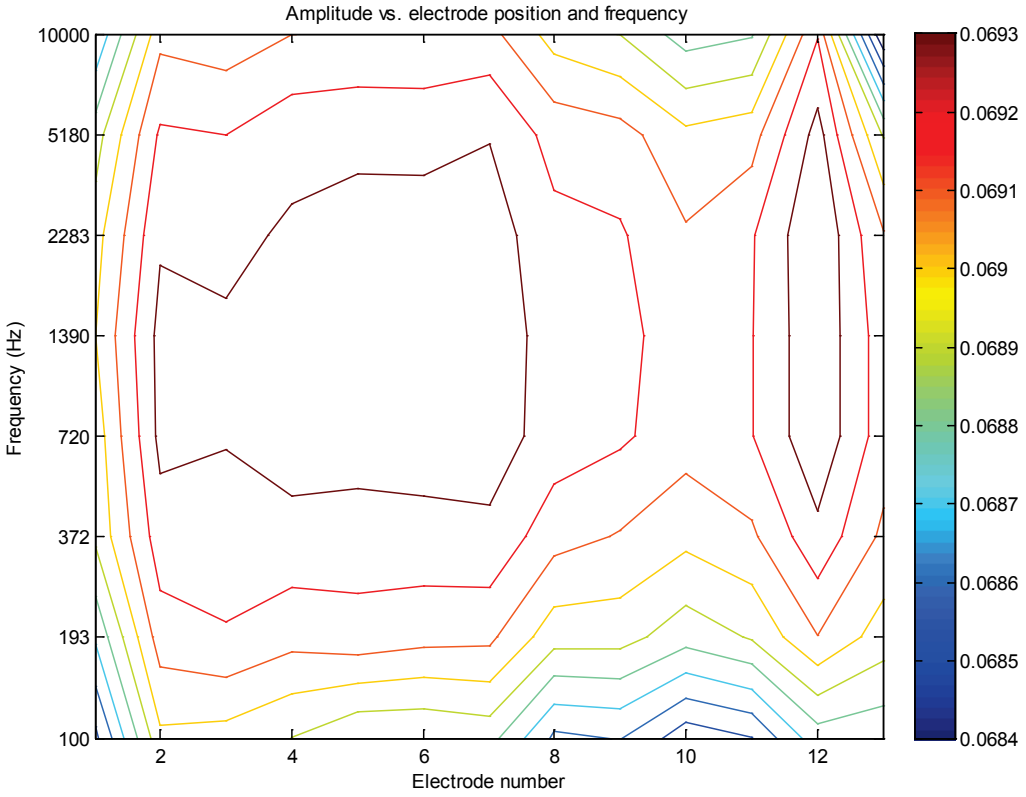

Figure 5-15: Contour plot indicating presence of cells at electrode pairs 2, 3, 4, 5, 6, 7 and 12

It was also verified that when the frequency of measurement was high (100 kHz and above), the signal dropped significantly as shown in the frequency sweep graph, Figure 5-16. Hence, lower frequency range was selected for the next set of experimentation.

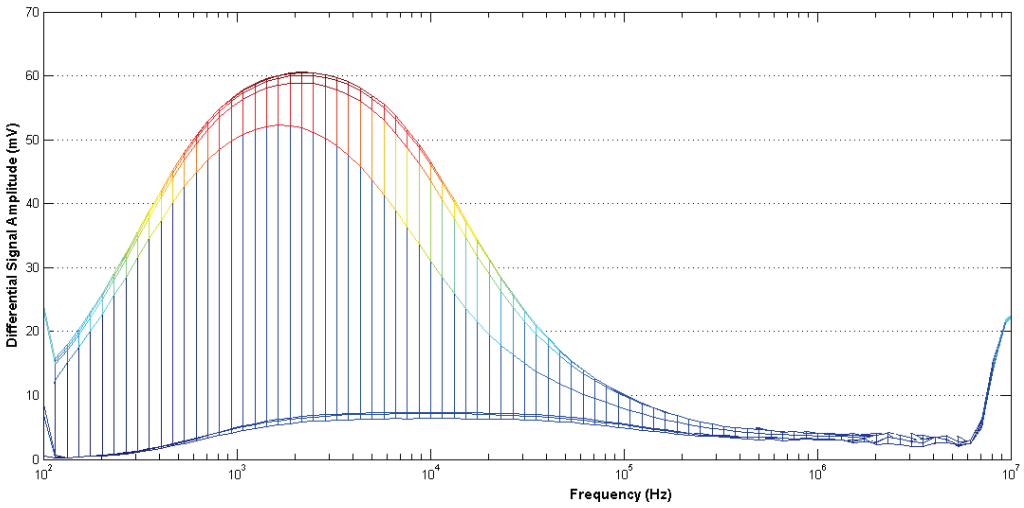

Figure 5-16: Frequency sweep across the 14 pair of electrode pairs showing signal drop at higher frequencies

5.3.4. Results with E-Coli bacteria

The final set of measurements was done by culturing E-Coli bacteria on an agar film and monitoring the electrical impedance over time. As shown in Figure 5-17, there were no visible bacterial colonies at this time. A control biosensor chip was also used in parallel with the biosensor as a reference. This control chip does not have any bacteria cultures on top of the agar film; it only contains agar film on top on the electrodes (Figure 5-19).

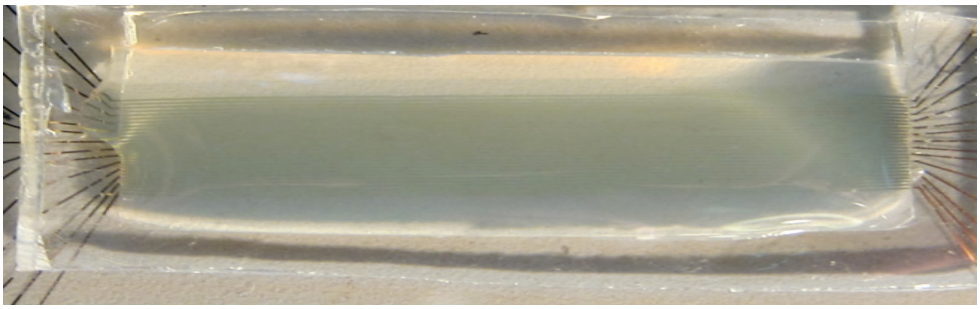

Figure 5-17: Top of the pathogen detection biosensor at time t=0

Figure 5-18 shows the initial signal measurement taken at time t=0. The slight variation in the signal amplitude is assumed to be because of the non-uniform agar layer on top of the electrodes.

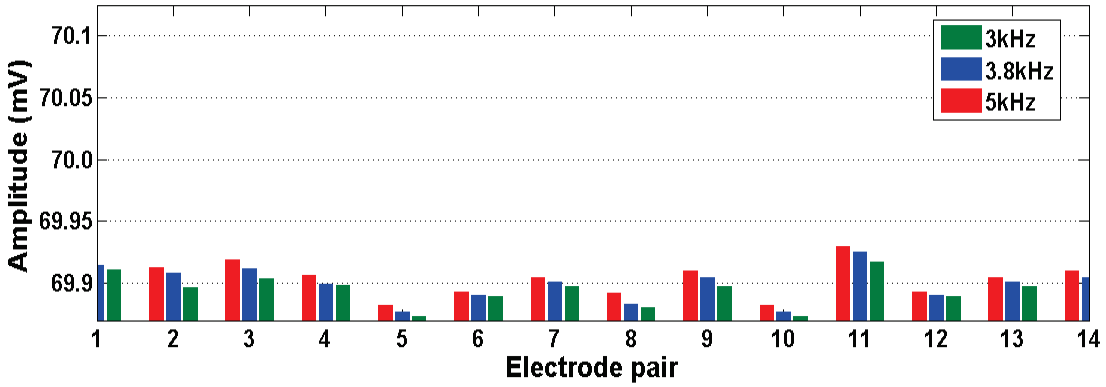

Figure 5-18 : Signal amplitude over the electrode pairs for pathogen detection biosensor at time t=0 at different frequencies

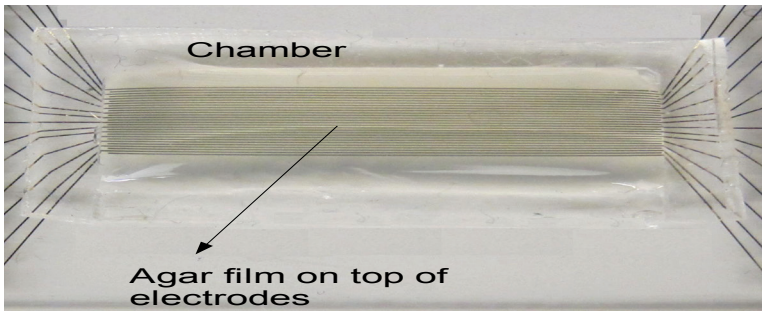

Figure 5-19 : Top of the control biosensor chip used as a reference at time t=0

Signal amplitude was measured over the electrode pairs for the control biosensor chip as shown in Figure 5-20.

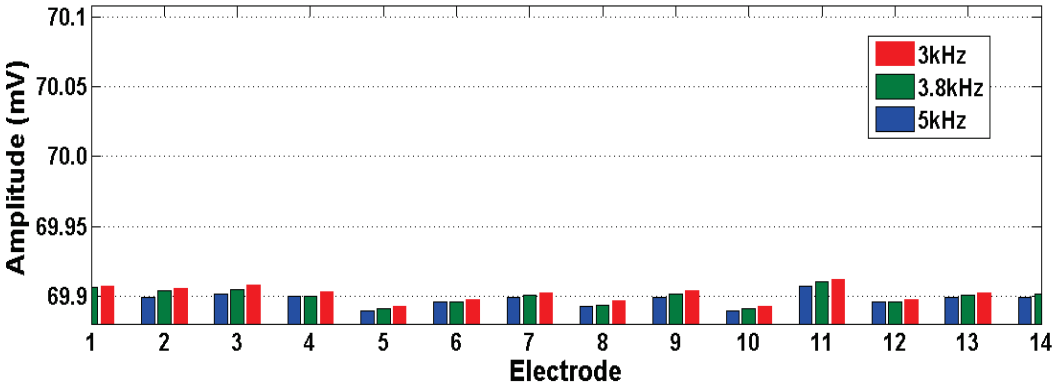

Figure 5-20: Signal amplitude over the electrode pairs for the control biosensor at time t=0 at different measurement frequencies

Data was recorded over time for all the electrode pairs for three frequencies viz. 3 kHz, 3.8 kHz and 5 kHz and no change in the signal was observed for the first seven hours. After 8 hours, there was an increase of 0.12 mV in the signal amplitude over electrode pair #3 and 0.24 mV increase over electrode pair#7 as shown in Figure 5-21.

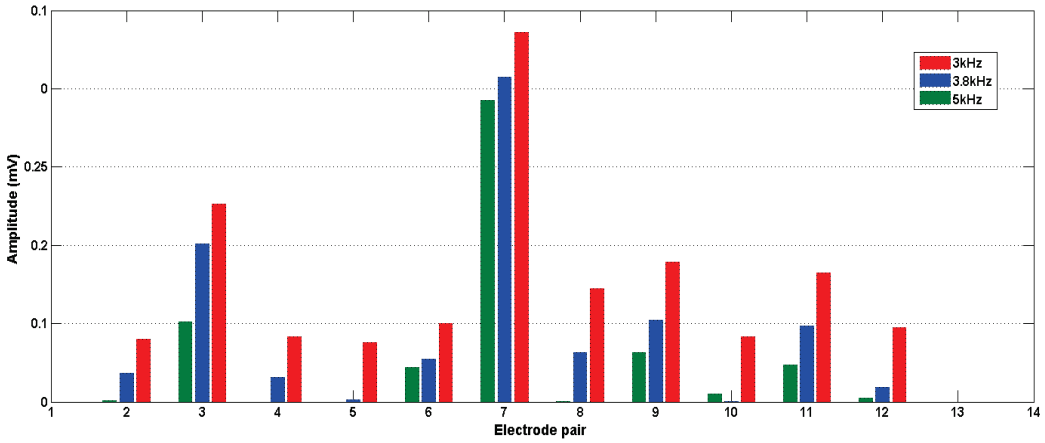

Figure 5-21: Signal amplitude over the electrode pairs at time t = 8 hours

As shown in Figure 5-22, no change in signal was observed over the control biosensor. However, there was no visible growth of bacteria on the top of the agar film on both the pathogen detection biosensor as well the control biosensor.

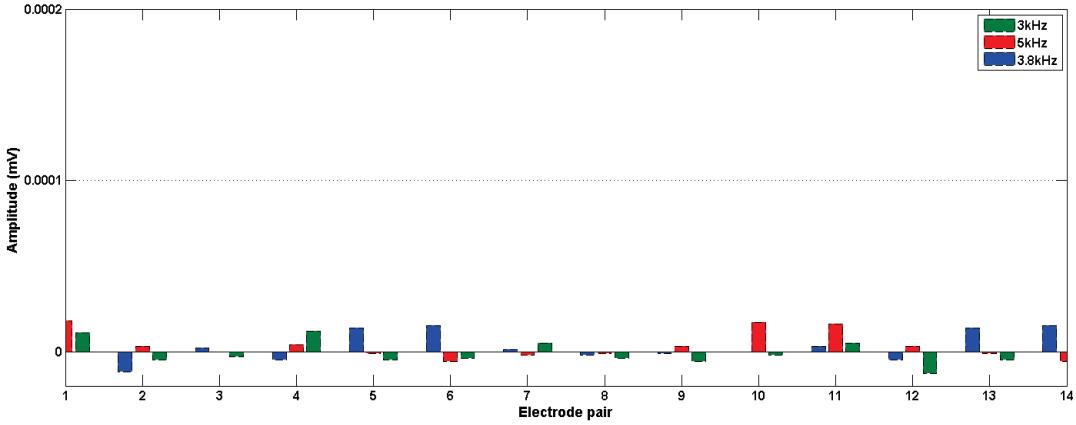

Figure 5-22: Signal amplitude measurement over the electrode pairs for the control biosensor at time t=8 hours

After 10 hours, there were barely visible colonies over the electrodes 2 and 7 on the top of the agar medium of pathogen detection biosensor as shown in Figure 5-23.

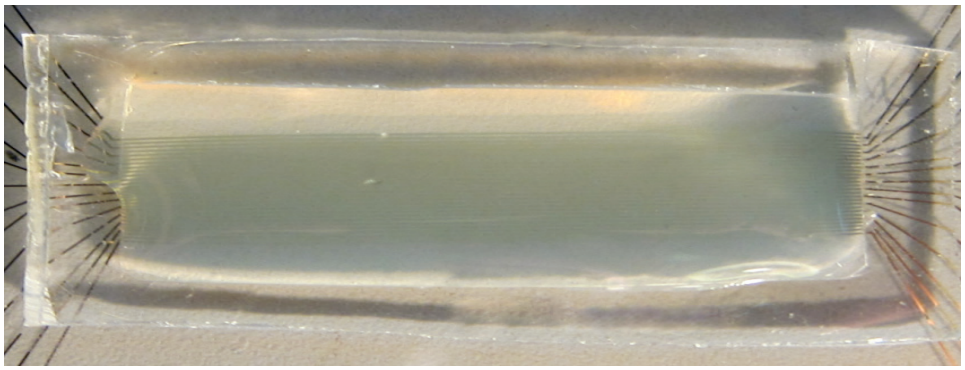

Figure 5-23: Partially visible colonies over electrode pairs 2 and 7 on pathogen detection biosensor chip at t=10 hours

The signal variation at this time is as shown in the Figure 5-24.

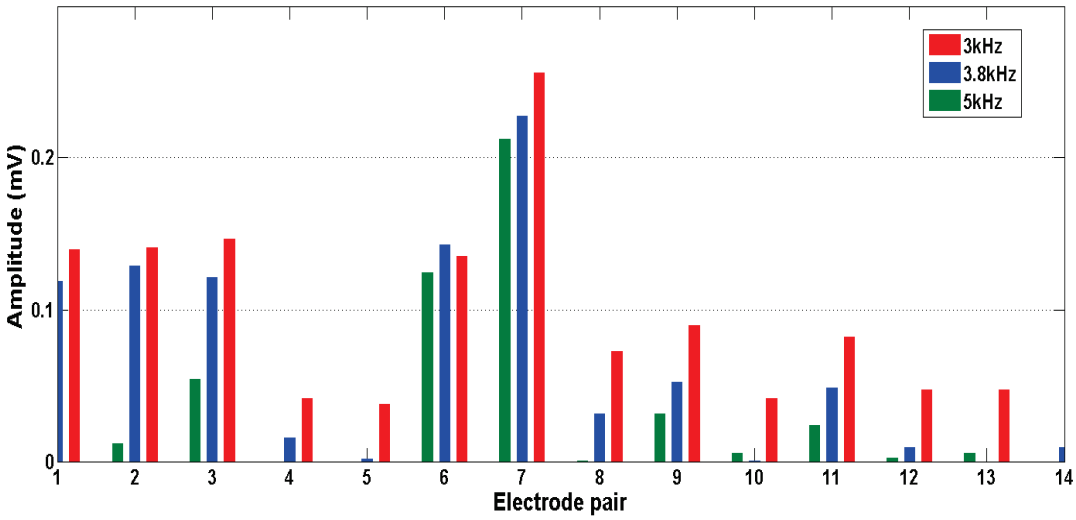

Figure 5-24: Signal amplitude measurements across the 14 pair of electrodes after t=10 hours

It was obsevered that with the passage of time the size of the colonies over the electrodes pairs 1,2,3 and 6,7,8 increased and thereby the measured signal also increased across these electrode pairs.

The variation in impedance after 12 hours and 16 hours is as shown in figure 5-26 and 5-27 respectively. The top of the bisosensor chip picture is as shown in figure 5-25 and figure 5-27 for time 12 hours and 16 hours respectively.

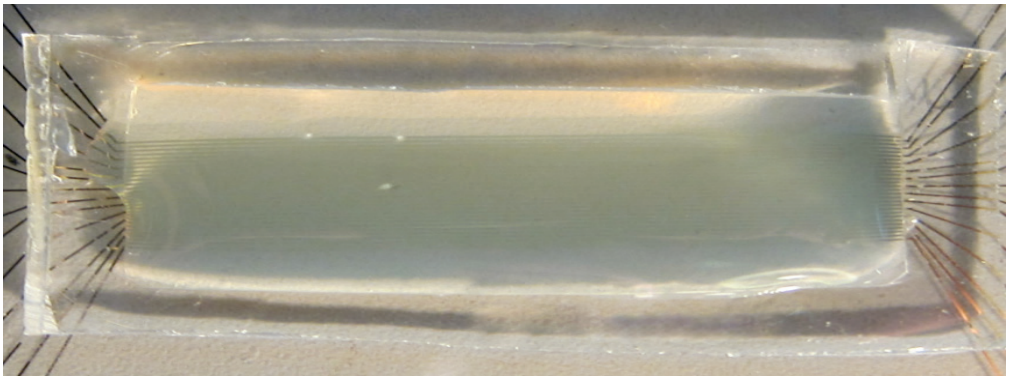

Figure 5-25: Bacteria growth on the top of the agar film after 12 hours

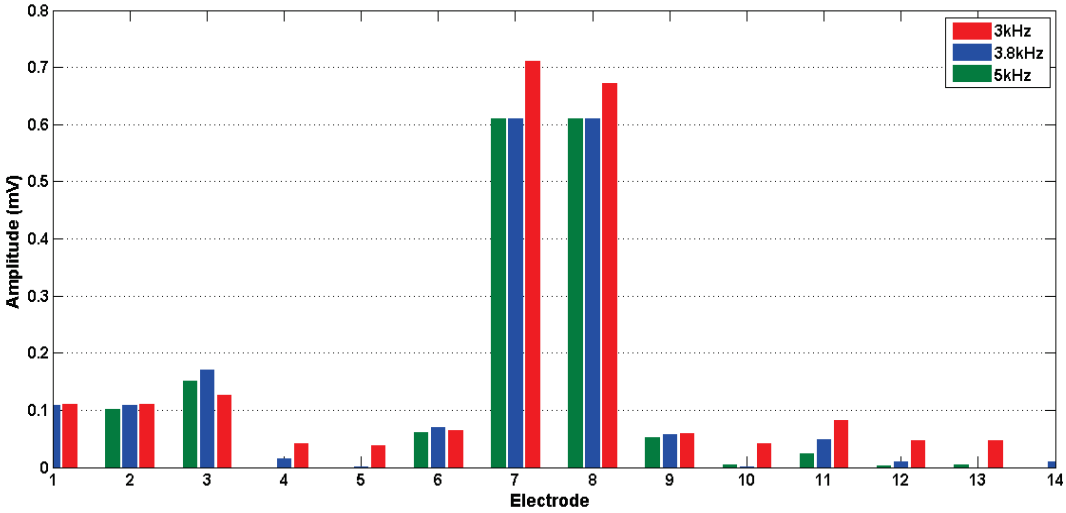

Figure 5-26: Signal amplitude measurements across the 14 pair of electrodes after t=12 hours

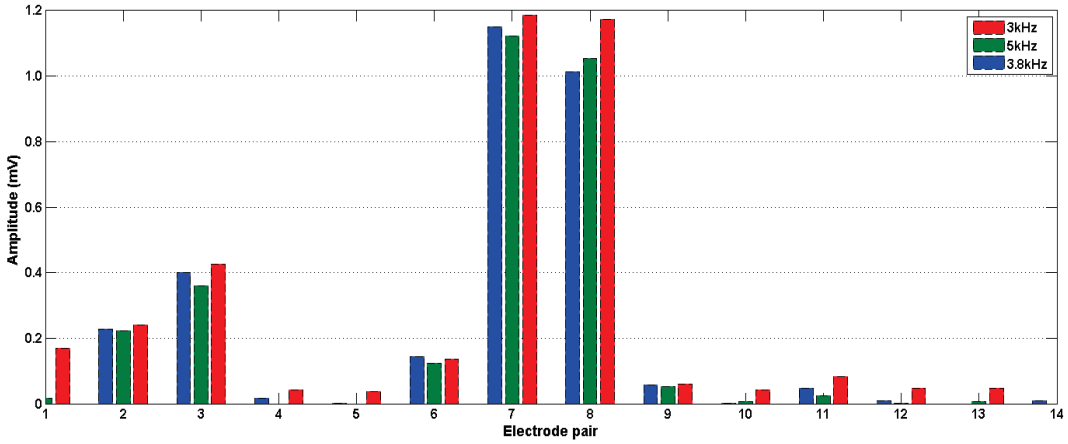

Figure 5-27: Signal measurements across the 14 pair of electrodes after t=16 hours

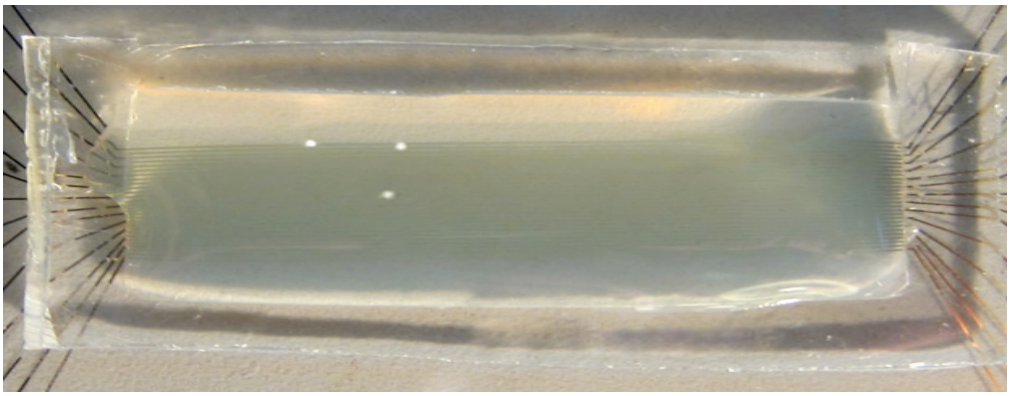

Figure 5-28: Bacteria growth on the top of the agar film after 16 hours

The variation of signal amplitude for the pathogen detection biosensor chip and the control biosensor chip over a time period of 24 hours across electrode pair 7 is as shown in figure 5-28. The biosensor chip after 24 hours is as shown in figure 5-29.

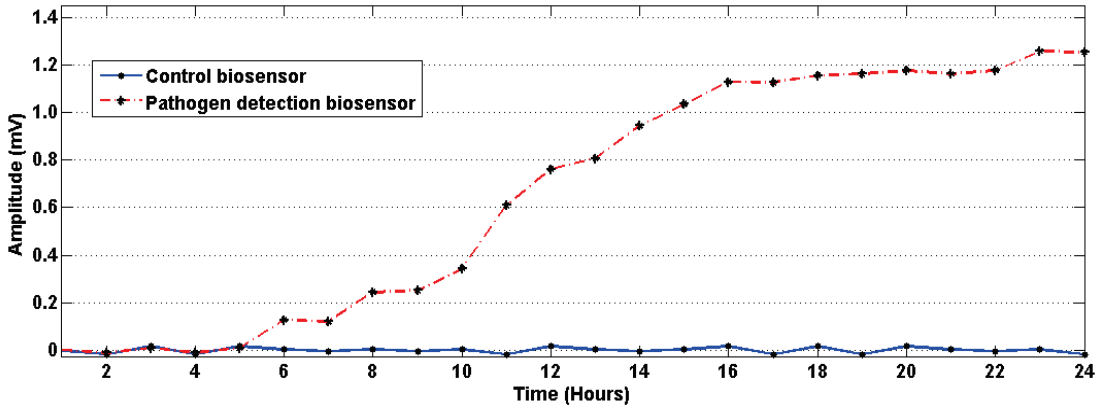

Figure 5-29: Variation of signal between electrodes 7 over time for pathogen detection biosensor chip and control biosensor chip over 24 hours

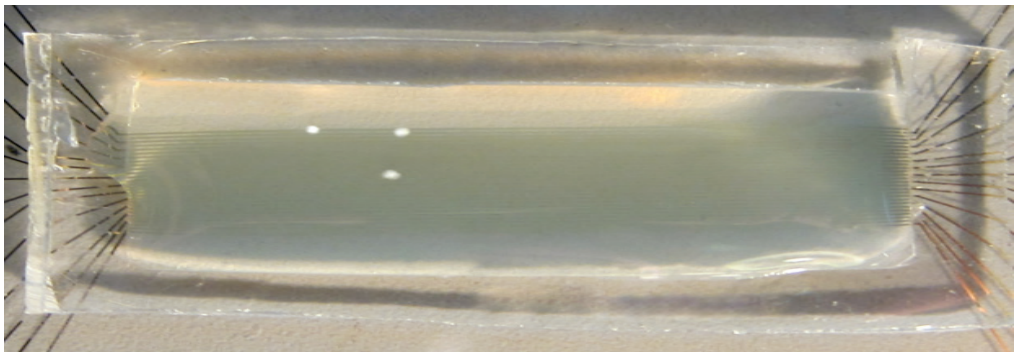

Figure 5-30: Pathogen detection biosensor chip showing the growth of bacteria after 24 hours

Figure 5-31 clearly compared the change in signal amplitude for time 0 hours and 24 hours for both the pathogen detection biosensor and the control biosensor.

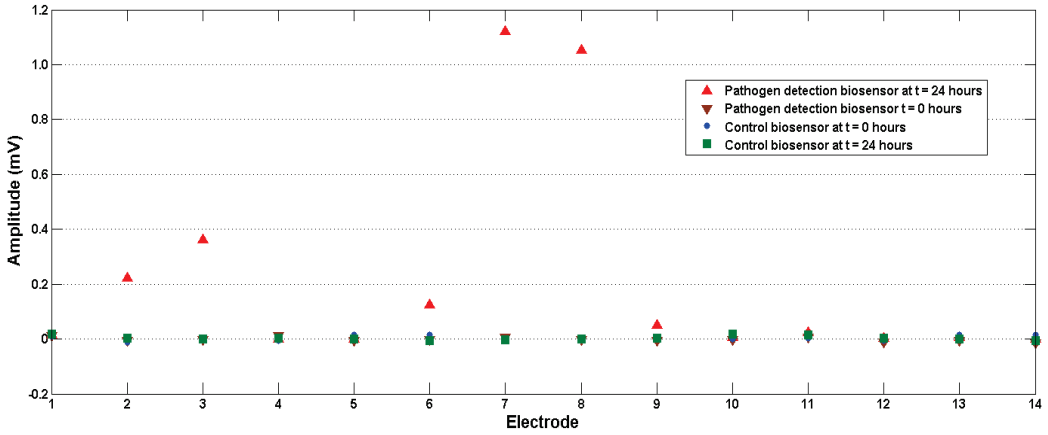

Figure 5-31: Signal amplitude comparison for pathogen detection biosensor and control biosensor at 0 hours and 24 hours

There was no signal change for the control biosensor used as a reference (as shown in figure 5-33) even after 24 hours justifying that the signal difference observed over some electrodes in the other biosensor was due to the growth of the bacteria over them. The control biosensor chip after a time period of 24 hours is as shown in figure 5-32. It was found that there was amplitude difference of 1.2mV across the electrode #7 where the bacteria was cultured compared to the ones with no bacteria. The detection of the presence of bacteria could be estimated after approximately 8-10 hours.

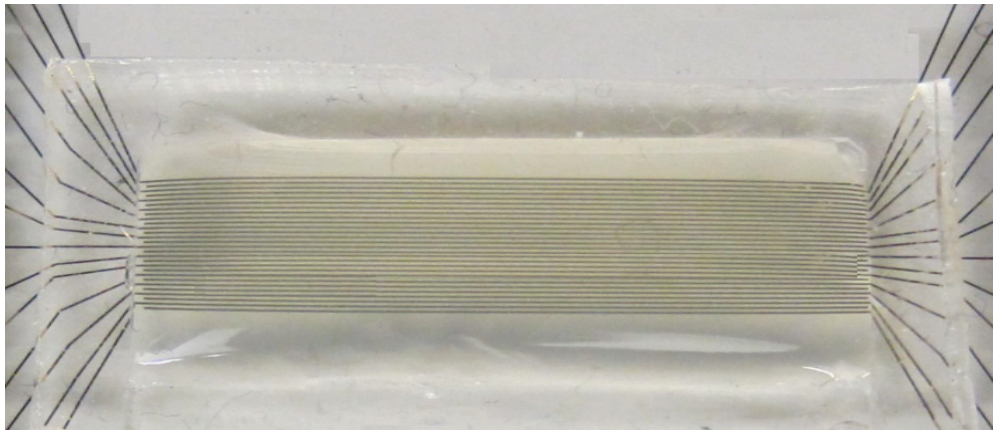

Figure 5-32 : Control biosensor chip showing no growth of bacteria after 24 hours

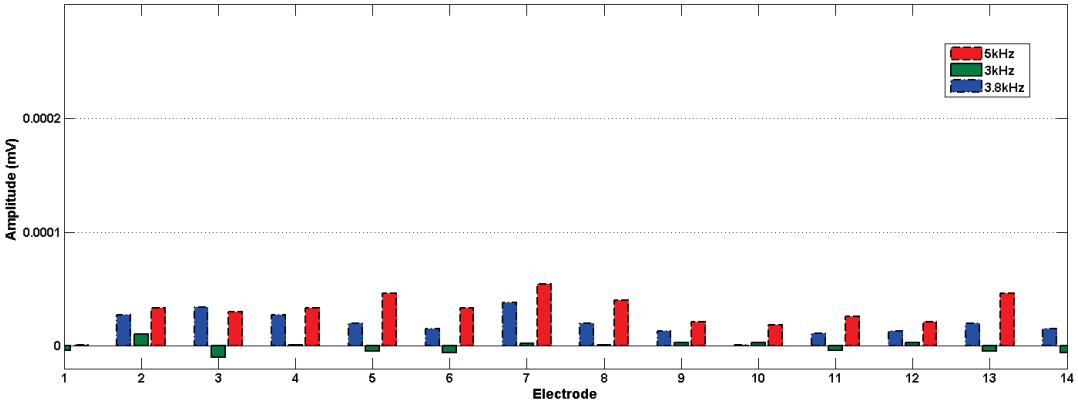

Figure 5-33 : Signal amplitude variation for the control biosensor after 24 hours

5.3.5. Challenges

There were a few challenges during this research. Firstly, during the fabrication stage the standard gold etchant caused huge undercuts leading to peeling off the electrodes. Therefore, aqua regia (3 parts of hydrochloric acid and one part of nitric acid) was used to etch gold electrodes.

Culturing of bacteria over these electrodes was another area of challenge. The agar layer deposited was about 1mm, which is one-third of the layer thickness of what is

normally used for culturing bacteria in a petri dish. This was to ensure easy detection of the cells culturing on the top of the agar layer. This thin layer had to be almost uniform free from any bumps. This agar layer was too thin, so it dried up due to heat inside the oven, hindering the culturing of bacteria. Therefore, the biosensor was kept inside a petri dish. Damped paper towels were kept on the sides of the container in order to maintain moisture.

6. Conclusions and future work

This thesis described the design, fabrication and testing of electrical biosensors for real time monitoring of bio-samples. Electrical detection techniques are comparatively less expensive and does not require any special labelling step as needed for optical based detection techniques. A microelectrode system was developed for detecting the bio-samples and tested using impedance measurement technique, and the results were seen as change in the impedance signal with variation in the properties of the bio-sample with time.

The first part of the thesis a comprehensive simulation model for a microfluidic device for dosage planning for a given cell was presented. Three key parts of the models included injection of a sample plug of a drug into the microchannel, correlation of the concentration profile of the drug to impedance, and electrical detection of the state of a cell. The finite element simulations were done using COMSOL. The finite element analysis helped us in the estimation of the geometry for the sensors developed. It was also useful to determine the flow profile, flow velocities and gave us a basic idea of the sensitivity of the electrical sensor towards the various samples under test.

A complete fabrication process for the microfluidic device was also discussed. SU-8 on silicon wafers were used to create the microchannel and chrome (Cr) and gold (Au) were used for patterning the electrodes on glass substrate. SU-8 is cost-effective for creating high-aspect microstructures and provides a good biocompatibility. The individual components were bonded together using reactive ion etching.

The first sensor utilized in this research was an electrical based chemical sensor. It lets us measure the variation in drug concentration, in real-time with high precision. Electrical properties were monitored continuously over the set of microelectrodes. Change in impedance was recorded due to the change in the concentration of the drug plug as it moved along a microchannel while it diffused into the buffer solution. One

electrode was excited with a sinusoidal voltage, and the conduction current was measured (converted to a voltage through a 50Ω resistor) for various concentrations of drug sample. However, for low drug concentrations, majority of conduction current was through the buffer which deteriorated the measurement accuracy. To circumvent this problem, real time differential measurements were taken across two sets of electrodes where the additional set of electrodes was kept in the buffer solution, enabling us to measure drug concentration of 10pMol/mL. This detection set up can be used to in many drug delivery and discovery applications and cell viability studies.

The second sensor was based on the same detection principle as used for the first sensor. Instead of array of electrodes it was designed to have set of interdigitated microelectrodes. The experimental set used was similar to the one used for the first sensor except that had an additional switching circuit. This switching circuit enabled us to make electrical measurements over the multiple electrode pairs simultaneously. Thereby, software setup was used featuring Matlab to handle timer, file IO, serial communication, data polling from the lock-in amplifier and user interfacing. As mentioned before, conduction current was measured across all the electrodes while cells were incubated over the electors in a microchamber for 24 hours with time interval of 30 min. Peaks were observed across those electrodes where there was cell growth, whereas the signal was constant at other electrode areas. This thus helped in the detection of the cells as they culture over the agar film through electrical measurements. This research addresses the target area of biomedical technologies, by integrating molecular biochemistry, analytical biochemistry, and microfluidic engineering.

6.1. Future work

During the course of the work explained in this thesis, several possible process improvements were identified for future work. Future improvements can be separated into two main categories: develop a device that can be reused for detection of pathogens and improvements related to the design of the biosensors developed.

The first sensor utilized in this research reports the real time measurement of minute variations in drug concentration. The real-time differential measurements let us measure the local drug concentration with accuracies of better than 10pMol/mL.

However, no direct application of the device has been reported. Monitoring and determining the minute concentration is essential for many drug delivery and discovery applications. Recent advancement in these studies of drug development is for cardiovascular diseases. The mechanical response of a single cardiomyocyte to various drug concentrations is to be measured. This method requires delivering a specific dose of the drug over a short period of time while measuring the forces exerted by a cell that is kept inside a microchamber. However, the exact drug dosage is difficult to control for rapid variations in drug concentration, which hinders the accuracy of the measurements. Thus, the reported highly accurate measurement technique can be used for this application. Also, all the array of electrodes could be utilized to study the concentration profile of the drug by utilizing the switching circuit as studied and analysed in finite element simulations. This could give us a wider view of the drug profile variation and would be useful for the placement of cells in the microfluidic channel depending upon the drug concentration it is to be exposed.

The second biosensor reported helps us to detect the presence of cells as they culture on a thin agar film. After each measurement procedure, the electrodes and the PDMS cell chamber were to be cleaned with IPA and DI water. A new design can be proposed which can help to eliminate the cleaning process and also makes the electrical biosensor reusable. The electrodes could be placed at the bottom of the standard agar plate. This would decrease the effort of making a new chamber for culturing bacteria. This will also reduce the effort of preparing a thin layer of agar on the electrodes. For this, the electrodes should cover the entire agar circular plate. Although the present electrode design enabled us to detect the bacterial colonies but it was unable to count the bacterial colonies. The parallel electrode design can be modified to a mesh electrode design so that the measured signed can count of the number of colonies. A mesh electrode design, such as a grid, will provide us signal peaks for cell colonies growing across different electrode pair instead of giving an aggregate of the signal as in the case of parallel electrode design. This will allow us to count the number of localized colonies.

In the current work, gold microelectrodes are fabricated which will an expensive process for mass manufacture. Alternatively, ink-jet printing or screen printing manufacturing technique can be used to pattern the electrodes since it facilitates rapid,

reproducible and economical production for biosensors. This technique would be extremely versatile, and will enable a wide variety of reagents to be placed on virtually any sensor design. This technique will be particularly beneficial for the mass manufacture of complex devices, where existing production techniques, such as lithographic patterning, may not be suitable.

Throughout this research, lock in amplifier has been used to measure the change in impedance. Although, lock in amplifier had many advantages, but it is expensive equipment. Work can be done to make a set up to serve the same purpose as the lock-in amplifier that could be dedicated electronics to the present setup.

References

[1] B. Rashid, "BioMEMS: state-of-the-art in detection, opportunities and prospects," *Advanced Drug Delivery Reviews,* vol. 56, pp. 1565-1586, 2004.

[2] K. M. Ainslie and T. A. Desai, "Microfabricated implants for applications in therapeutic delivery, tissue engineering, and biosensing," *Lab on a Chip,* vol. 8, 2008.

[3] J.-L. Mas et al "Endarterectomy Versus Angioplasty in Patients with Symptomatic Severe Carotid Stenosis (EVA-3S) trial: results up to 4 years from a randomised, multicentre trial," *The Lancet Neurology,* vol. 7, pp. 885-892, 2008.

[4] M. J. Loeffelholz, D. L. Pong, R. B. Pyles, Y. Xiong, A. L. Miller, K. K. Bufton, and T. Chonmaitree, " Comparison of the filmarray respiratory panel and prodesse real-time pcr assays for the detection of respiratory pathogens," *Journal of Clinical Microbiology,* 2011.

[5] B. Toye, W. Woods, M. Bobrowska, and K. Ramotar, "Inhibition of PCR in Genital and Urine Specimens Submitted for Chlamydia trachomatis Testing," *Journal of Clinical Microbiology,* vol. 36, pp. 2356-2358, 1998.

[6] M. A. Hulten, S. Dhanjal, and B. Pertl, "Rapid and simple prenatal diagnosis of common chromosome disorders: advantages and disadvantages of the molecular methods FISH and QF-PCR," *Reproduction,* vol. 126, pp. 279-297, 2003.

[7] J.-H. Maeng, B.-C. Lee, Y.-J. Ko, W. Cho, Y. Ahn, N.-G. Cho, S.-H. Lee, and S. Y. Hwang, "A novel microfluidic biosensor based on an electrical detection system for alpha-fetoprotein," *Biosensors and Bioelectronics,* vol. 23, pp. 1319-1325, 2008.

[8] S.-J. Park, T. A. Taton, and C. A. Mirkin, "Array-Based Electrical Detection of DNA with Nanoparticle Probes," *Science,* vol. 295, pp. 1503-1506, 2002.

[9] J. Wu, Y. Ben, and H.-C. Chang, "Particle detection by electrical impedance spectroscopy with asymmetric-polarization AC electroosmotic trapping," *Microfluidics and Nanofluidics,* vol. 1, pp. 161-167, 2005.

[10] G. Zheng, F. Patolsky, Y. Cui, W. U. Wang, and C. M. Lieber, "Multiplexed electrical detection of cancer markers with nanowire sensor arrays," *Nat Biotech,* vol. 23, pp. 1294-1301, 2005.

[11] N. Bao, J. Wang, and C. Lu, "Recent advances in electric analysis of cells in microfluidic systems," *Analytical and Bioanalytical Chemistry,* vol. 391, pp. 933-942, 2008.

[12] R. Bragos, E. Sarro, A. Fontova, A. Soley, J. Cairo, A. Bayes-Genis, and J. Resell, "Four Versus Two-Electrode Measurement Strategies for Cell Growing and Differentiation Monitoring Using Electrical Impedance Spectroscopy," in *Engineering in Medicine and Biology Society, 2006. EMBS '06. 28th Annual International Conference of the IEEE*, 2006, pp. 2106-2109.

[13] P. Linderholm, T. Braschler, J. Vannod, Y. Barrandon, M. Brouard, and P. Renaud, "Two-dimensional impedance imaging of cell migration and epithelial stratification," *Lab on a Chip,* vol. 6, pp. 1155-1162, 2006.

[14] S. M. Radke and E. C. Alocilja, "A high density microelectrode array biosensor for detection of E. coli O157:H7," *Biosensors and Bioelectronics,* vol. 20, pp. 1662-1667, 2005.

[15] A. C. Boccara, D. Fournier, and J. Badoz, "Thermo optical spectroscopy: Detection by the mirage effect," *Applied Physics Letters,* vol. 36, pp. 130-132, 1980.

[16] F. Foret, M. Deml, V. Kahle, and P. Boček, "On-line fiber optic UV detection cell and conductivity cell for capillary zone electrophoresis," *ELECTROPHORESIS,* vol. 7, pp. 430-432, 1986.

[17] A. Wolff, I. R. Perch-Nielsen, U. D. Larsen, P. Friis, G. Goranovic, C. R. Poulsen, J. P. Kutter, and P. Telleman, "Integrating advanced functionality in a microfabricated high-throughput fluorescent-activated cell sorter," *Lab on a Chip,* vol. 3, 2003.

[18] Q.-J. Li, A. R. Dinner, S. Qi, D. J. Irvine, J. B. Huppa, M. M. Davis, and A. K. Chakraborty, "CD4 enhances T cell sensitivity to antigen by coordinating Lck accumulation at the immunological synapse," *Nat Immunol,* vol. 5, pp. 791-799, 2004.

[19] S. Wee, G. L. Schieven, J. M. Kirihara, T. T. Tsu, J. A. Ledbetter, and A. Aruffo, "Tyrosine phosphorylation of CD6 by stimulation of CD3: augmentation by the CD4 and CD2 coreceptors," *The Journal of Experimental Medicine,* vol. 177, pp. 219-223, 1993.

[20] A. Y. Fu, H.-P. Chou, C. Spence, F. H. Arnold, and S. R. Quake, "An Integrated Microfabricated Cell Sorter," *Analytical Chemistry,* vol. 74, pp. 2451-2457, 2002/06/01 2002.

[21] D. P. Schrum, C. T. Culbertson, S. C. Jacobson, and J. M. Ramsey, "Microchip Flow Cytometry Using Electrokinetic Focusing," *Analytical Chemistry,* vol. 71, pp. 4173-4177, 1999/10/01 1999.

[22] H. E. Ayliffe, A. B. Frazier, and R. D. Rabbitt, "Electric impedance spectroscopy using microchannels with integrated metal electrodes," *Microelectromechanical Systems, Journal of,* vol. 8, pp. 50-57, 1999.

[23] T. B. Jones, "Electromechanics of Particles," ed Cambridge Cambridge University Press, 1995.

[24] H. a. G. Morgan, N.G., *AC Electrokinetics: Colloids and Nanoparticles*. Philadelphia, PA, USA: Research Studies Press, 2003.

[25] E. Gheorghiu and K. Asami, "Monitoring cell cycle by impedance spectroscopy: experimental and theoretical aspects," *Bioelectrochemistry and Bioenergetics,* vol. 45, pp. 139-143, 1998.

[26] K. Asami, T. Yonezawa, H. Wakamatsu, and N. Koyanagi, "Dielectric spectroscopy of biological cells," *Bioelectrochemistry and Bioenergetics,* vol. 40, pp. 141-145, 1996.

[27] K. Asami, Y. Takahashi, and S. Takashima, "Dielectric properties of mouse lymphocytes and erythrocytes," *Biochimica et Biophysica Acta (BBA) - Molecular Cell Research,* vol. 1010, pp. 49-55, 1989.

[28] W. Coulter, "Means for counting particles suspended in a fluid," US Patent 656, 1949.

[29] U. D. Larsen, G. Blankenstein, and J. Branebjerg, "Microchip Coulter particle counter," in *Solid State Sensors and Actuators, 1997. TRANSDUCERS '97 Chicago., 1997 International Conference on*, 1997, pp. 1319-1322 vol.2.

[30] M. Koch and et al., "Design and fabrication of a micromachined Coulter counter," *Journal of Micromechanics and Microengineering,* vol. 9, p. 159, 1999.

[31] Fuller, C. K, Hamilton, J., Ackler, H. and Gascoyne, P. R. C.," In Microfabricated Multi frequency Particle Impedance Characterization System, "Proceedings of Micro Total Analysis Systems, Enschede, Netherlands, pp. 265-268, 2000.

[32] Larsen, U. D.,Norring,H. andTelleman,P. "In Somatic Cell counting with Silicone Apertures, " Proceedings of Micro Total Analysis Systems, Enschede, Netherlands pp. 103-106.,2000

[33] S. Gawad, M. Henschkel, Y. Leung-Ki, R. Iuzzolino, L. Schild, P. Lerch, and P. Renaud, "Fabrication of a microfluidic cell analyzer in a microchannel using impedance spectroscopy," in Mic*rotechnologies in Medicine and Biology, 1st Annual International, Conference On. 2000, 2*000, pp. 297-301.

[34] W. Franks, I. Schenker, P. Schmutz, and A. Hierlemann, "Impedance characterization and modeling of electrodes for biomedical applications," Bio*medical Engineering, IEEE Transactions on, vol*. 52, pp. 1295-1302, 2005.

[35] E. T. McAdams, A. Lackermeier, J. A. McLaughlin, D. Macken, and J. Jossinet, "The linear and non-linear electrical properties of the electrode-electrolyte interface," Bio*sensors and Bioelectronics, vol*. 10, pp. 67-74, 1995.

[36] B. Wessling, W. Mokwa, and U. Schnakenberg, "RF-sputtering of iridium oxide to be used as stimulation material in functional medical implants," Jou*rnal of Micromechanics and Microengineering, vol*. 16, p. S142, 2006.

[37] S. Gawad, K. Cheung, U. Seger, A. Bertsch, and P. Renaud, "Dielectric spectroscopy in a micromachined flow cytometer: theoretical and practical considerations," Lab *on a Chip, vol*. 4, pp. 241-251, 2004.

[38] G. Mernier, W. Hasenkamp, N. Piacentini, and P. Renaud, "Multiple-frequency impedance measurements in continuous flow for automated evaluation of yeast cell lysis," Sen*sors and Actuators B: Chemical,* http://www.sciencedirect.com/science/article/pii/S0925400510008683, 4 November 2010.

*[*39] Braschler T., " Single Cell Positining , Entrapment and Electrical Characterisation, " Proceedings of the Ninth International Conference on Miniaturized Systems for chemistry and Life Sciences pp2-4 ,2005.

[40] C. Kaittanis, S. Santra, and J. M. Perez, "Emerging nanotechnology-based strategies for the identification of microbial pathogenesis," Adv*anced Drug Delivery Reviews, vol*. 62, pp. 408-423, 2010.

[41] Y. Yang, H. Zhang, J. Zhu, G. Wang, T.-R. Tzeng, X. Xuan, K. Huang, and P. Wang, "Distinguishing the viability of a single yeast cell with an ultra-sensitive radio frequency sensor," Lab *on a Chip, vol*. 10, pp. 553-555, 2010.

[42] C. Gershome, E. Lin, H. Kashihara, L. Hove-Madsen, and G. F. Tibbits, "Colocalization of voltage-gated Na+ channels with the Na+/Ca2+ exchanger in rabbit cardiomyocytes during development," Ame*rican Journal of Physiology - Heart and Circulatory Physiology, vol*. 300, pp. H300-H311, 2011.

[43] D. Di Carlo, N. Aghdam, and L. P. Lee, "Single-Cell Enzyme Concentrations, Kinetics, and Inhibition Analysis Using High-Density Hydrodynamic Cell Isolation Arrays," Ana*lytical Chemistry, vol*. 78, pp. 4925-4930, 2006/07/01 2006.

[44] Comsol version 3.5a ,Retrieved (10/ 20/ 2010), from www.uk.comsol.com: http://www.uk.comsol.com/shared/downloads/products/releasenotes_35a.pdf, 2010

[45] B. Srinivasan, "Simulation of an Electrical Impedance Based Microfluidic Biosensor for Detection of E.coli Cells," presented at the The Proceedings of the COMSOL Users Conference, Boston, 2006.

[46] Y. S. Fung and Y. Y. Wong, "Self-Assembled Monolayers as the Coating in a Quartz Piezoelectric Crystal Immunosensor To Detect Salmonella in Aqueous Solution," Ana*lytical Chemistry, vol*. 73, pp. 5302-5309, 2001/11/01 2001.

[47] V. Koubová, E. Brynda, L. Karasová, J. Škvor, J. Homola, J. Dostálek, P. Tobiška, and J. Rošický, "Detection of foodborne pathogens using surface plasmon resonance biosensors," Sen*sors and Actuators B: Chemical, vol*. 74, pp. 100-105, 2001.

[48] R. Gómez, R. Bashir, and A. K. Bhunia, "Microscale electronic detection of bacterial metabolism," Sen*sors and Actuators B: Chemical, vol*. 86, pp. 198-208, 2002.

[49] K. G. Ong, J. Wang, R. S. Singh, L. G. Bachas, and C. A. Grimes, "Monitoring of bacteria growth using a wireless, remote query resonant-circuit sensor: application to environmental sensing," Bio*sensors and Bioelectronics, vol*. 16, pp. 305-312, 2001.

[50] H. Li and R. Bashir, "Dielectrophoretic separation and manipulation of live and heat-treated cells of Listeria on microfabricated devices with interdigitated electrodes," Sen*sors and Actuators B: Chemical, vol*. 86, pp. 215-221, 2002.

[51] G. H. Markx and C. L. Davey, "The dielectric properties of biological cells at radiofrequencies: applications in biotechnology," Enz*yme and Microbial Technology, vol*. 25, pp. 161-171, 1999.

[52] D. Voltmer, "Fundamentals of Electromagnetics 2. Synthesis lectures on computational electromagnetics," Syn*thesis Lectures on Computational Electromagnetics, vol*. 15, pp. 1-217, 2007.

[53] T. Lanz, S. Hafizovic, J. Rothe, R. Streichan, N. Goedecke, F. Heer, and A. Hierlemann, "Differential impedance spectrometer and vision system for analysis of single cells," in Sol*id-State Sensors, Actuators and Microsystems Conference, 2009. TRANSDUCERS 2009. International, 2*009, pp. 1297-1300.

[54] P. Renaud, H. van Lintel, M. O. Heuschkel, L. Guerin, D. J. Harrison, and A. van den Berg, "Photo-polymer microchannel technologies and applications," presented at the 3rd International Symposium on Micro-Total Analysis Systems (MU-TAS'98), BANFF, CANADA, 2000.

[55] B. H. Jo, L. M. Van Lerberghe, K. M. Motsegood, and D. J. Beebe, "Three-dimensional micro-channel fabrication in polydimethylsiloxane (PDMS) elastomer," Mic*roelectromechanical Systems, Journal of, vol*. 9, pp. 76-81, 2000.

[56] C. Luo, F. Meng, X. Liu, and Y. Guo, "Reinforcement of a PDMS master using an oxide-coated silicon plate," Mic*roelectronics Journal, vol*. 37, pp. 5-11, 2006.

[57] S. Bhattacharya, A. Datta, J. M. Berg, and S. Gangopadhyay, "Studies on surface wettability of poly(dimethyl) siloxane (PDMS) and glass under oxygen-plasma treatment and correlation with bond strength," Mic*roelectromechanical Systems, Journal of, vol*. 14, pp. 590-597, 2005.

[58] K. Haubert, T. Drier, and D. Beebe, "PDMS bonding by means of a portable, low-cost corona system," Lab *on a Chip, vol*. 6, 2006.